Abstract

Acousto-optics science deals with the interaction between sound and light waves. Acousto-optic waves are most important in transferring signals through the communication systems, since modulating signals takes a great advantages in the field of communication engineering, bio-medical, laser beam deflection and laser intensity modulation.

The aim of this work is to simulate the fundamentals of an Acousto-Optic Modulator. The simulation procedure is based on theoretical and computational relationships describing acousto-optic properties for three selected materials which are “Glass, Germanium, and Tellurium-Oxide”. Two computer programs have been written using “MATLAB” software, the first used to verify the normalized intensity of the diffracted orders versus peak phase delay using partial differential equation, while the second program is used to study the normalized intensity of the electric field versus time wave propagation and electro-magnetic wave propagation in x, y and z directions, using Finite Difference Time Domain. The results for Glass and Tellurium-Oxide materials shows that the periodic exchange of the normalized intensity between the zero and first orders becomes smaller as the interaction length D increase, this indicate that the higher orders may appear very clear in these materials. The results for the Glass material show that the normalized intensity of the electric field increases with increasing electromagnetic wave propagation in x, y and z directions.

The results for Germanium shows that the peak intensity exchange for the zero diffracted order vanish quickly and coincidence with the higher diffracted orders.

Acknowledgement

I must first thank ALLAH for helping me to complete this study.

I thank my Supervisors Prof. Dr. Ayad A. Al-Ani and Dr. Ahmad Kamal for their valued information and supports to complete this thesis.

Special thanks to Mr. Omar Ayad for his big efforts for helping me in this thesis.

I want to thank all my family for their encouragements and support; the thanks extend to all my friends and colleagues for any provided assistance.

Marwa Kamal Mustafa

APPENDIX-A

Flow chart program use for calculating intensity of the diffracted orders versus peak phase delay in MATLAB

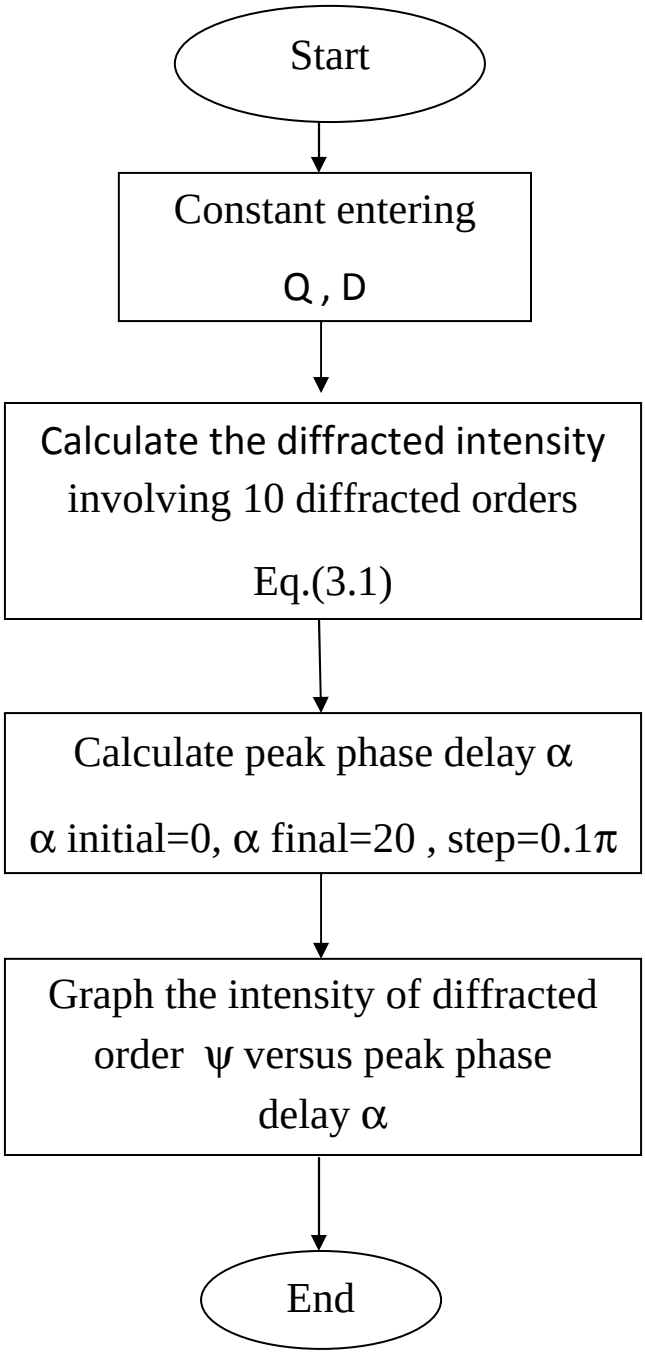

APPENDIX-B

Flow chart program use for calculating intensity of the electric field versus time propagation and electro magnetic wave propagation in MATLAB

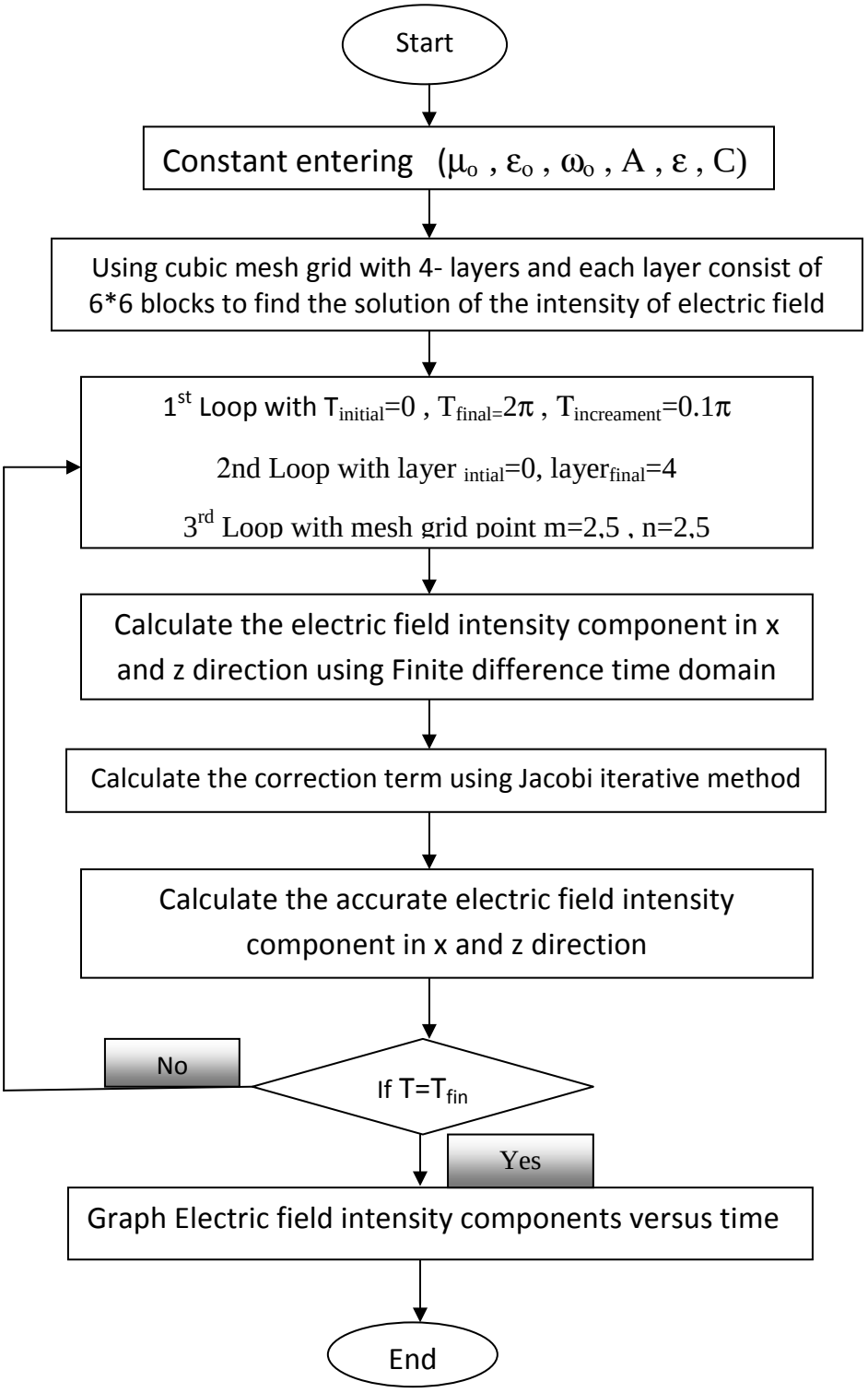

APPENDIX-C

The intensity of the electric field term in x and z direction using Jacobi iterative formula can be shown as the following equations

$$Ex_{(n,m,LN)} = (\frac{1}{4}) * [Ex_{(n-1,m,LN-1)} + Ex_{(n+1,m,LN-1)} + Ex_{(n,m-1,LN-1)} + Ex_{(n,m+1,LN-1)}] \quad (1)$$

$$Ez_{(n,m,LN)} = \left(\frac{1}{4}\right) * [Ez_{(n-1,m,LN-1)} + Ez_{(n+1,m,LN-1)} + Ez_{(n,m-1,LN-1)} + Ez_{(n,m+1,LN-1)}] \quad (2)$$

$$Exm_{(n,m,LN)} = \left(\frac{1}{4}\right) * [Exme_{(n-1,m,LN-1)} + Exme_{(n+1,m,LN-1)} + Exme_{(n,m-1,LN-1)} + Exme_{(n,m+1,LN-1)}] \quad (3)$$

$$Ezm_{(n,m,LN)} = \left(\frac{1}{4}\right) * [Ezme_{(n-1,m,LN-1)} + Ezme_{(n+1,m,LN-1)} + Ezme_{(n,m-1,LN-1)} + Ezme_{(n,m+1,LN-1)}] \quad (4)$$

$$Exd_{(n,m,LN)} = \left(\frac{1}{4}\right) * [Exd_{(n-1,m,LN-1)} + Exd_{(n+1,m,LN-1)} + Exd_{(n,m-1,LN-1)} + Exd_{(n,m+1,LN-1)}] \quad (5)$$

$$Ezd_{(n,m,LN)} = \left(\frac{1}{4}\right) * [Ezd_{(n-1,m,LN-1)} + Ezd_{(n+1,m,LN-1)} + Ezd_{(n,m-1,LN-1)} + Ezd_{(n,m+1,LN-1)}] \quad (6)$$

The correction term for the electric field component in x and z direction can be introduced as the following equations

$$Ex_{(n,m,LN)} = Ex_{(n,m,LN)} - \left(\frac{1}{4}\right) * [Ex_{(n+1,m,LN)} - 2 * Ex_{(n,m,LN)} + Ex_{(n-1,m,LN)} + Ex_{(n,m+1,LN)} - 2 * Ex_{(n,m,LN)} + Ex_{(n,m-1,LN)}] \quad (7)$$

$$Ez_{(n,m,LN)} = Ez_{(n,m,LN)} - \left(\frac{1}{4}\right) * [Ez_{(n+1,m,LN)} - 2 * Ez_{(n,m,LN)} + Ez_{(n-1,m,LN)} + Ez_{(n,m+1,LN)} - 2 * Ez_{(n,m,LN)} + Ez_{(n,m-1,LN)}] \quad (8)$$

$$Exm_{(n,m,LN)} = Exm_{(n,m,LN)} - \left(\frac{1}{4}\right) * [Exm_{(n+1,m,LN)} - 2 * Exm_{(n,m,LN)} + Exm_{(n-1,m,LN)} + Exm_{(n,m+1,LN)} - 2 * Exm_{(n,m,LN)} + Exm_{(n,m-1,LN)}] \quad (9)$$

$$Ezm_{(n,m,LN)} = Ezm_{(n,m,LN)} - \left(\frac{1}{4}\right) * [Ezm_{(n+1,m,LN)} - 2 * Ezm_{(n,m,LN)} + Ezm_{(n-1,m,LN)} + Ezm_{(n,m+1,LN)} - 2 * Ezm_{(n,m,LN)} + Ezm_{(n,m-1,LN)}] \quad (10)$$

$$Exd_{(n,m,LN)} = Exd_{(n,m,LN)} - \left(\frac{1}{4}\right) * [Exd_{(n+1,m,LN)} - 2 * Exd_{(n,m,LN)} + Exd_{(n-1,m,LN)} + Exd_{(n,m+1,LN)} - 2 * Exd_{(n,m,LN)} + Exm_{(n,m-1,LN)}] \quad (11)$$

$$Ezd_{(n,m,LN)} = Ezd_{(n,m,LN)} - \left(\frac{1}{4}\right) * [Ezd_{(n+1,m,LN)} - 2 * Ezd_{(n,m,LN)} + Ezd_{(n-1,m,LN)} + Ezd_{(n,m+1,LN)} - 2 * Ezd_{(n,m,LN)} + Ezd_{(n,m-1,LN)}] \quad (12)$$

الخلاصه

علم الموجات الصوتيه-البصريه تتعامل مع التفاعل بين الموجات الصوتيه والضوئيه. الموجات الصوتيه-البصريه مهمه جدا في نقل الاشارات خلال انظمه الاتصالات, لذلك الاشارات المضمنه لها فوائد عظيمه في مجال هندسه الاتصالات والطب البايولوجي وانحراف حزمه الليزروشدة الليزر المضمنه. الهدف من هذا العمل هو بناء برنامج محاكاة لدراسة اساسيات التضمين الصوتي-البصري. تم بناء طريقه المحاكاة على اساس القاعدة النظريه والعلاقات الحسابيه التي تصف الخواص الصوتيه-البصريه لثلاث مواد مختارة وهي "الزجاج, الجرمانيوم و اوكسيد التريليوم". تم كتابه برنامجين باستعمال لغه "MATLAB", الاول يستعمل لاظهار المعيارية في الشدة لمراتب الحيود كدالة للفاصله الطوريه باستعمال المعادلات التفاضليه الجزئيه, بينما البرنامج الثاني يستعمل لدراسه المعيارية في شدة المجال الكهربائي كدالة لزمن انتقال الموجه وانتقال الموجه الكهرومغناطيسيه باتجاه المحاور الثلاثة بطريقه الفروقات المحددة لمجال الزمن. من خلال النتائج لمادتي الزجاج واوكسيد التريليوم تبين بان التغير الدوري للمعيارية في شدة مراتب الحيود بين المرتبه الصفريه والمرتبه الاولى تصبح صغيرة بزيادة طول التفاعل وهذا يشير الى ان مراتب الحيود الاعلى تبدو واضحه جدا في هذه المواد. النتائج لمادة الزجاج تبين بان المعيارية في شدة المجال الكهربائي تزداد مع انتقال الموجه الكهرومغناطيسيه باتجاه المحاور الثلاثة.

الخلاصه

علم الموجات الصوتيه-البصريه تتعامل مع التفاعل بين الموجات الصوتيه والضوئيه. الموجات الصوتيه-البصريه مهمه جدا في نقل الاشارات خلال انظمه الاتصالات, لذلك الاشارات المضمنه لها فوائد عظيمه في مجال هندسه الاتصالات والطب البايولوجي وانحراف حزمه الليزروشدة الليزر المضمنه. الهدف من هذا العمل هو بناء برنامج محاكاة لدراسة اساسيات التضمين الصوتي-البصري. تم بناء طريقه المحاكاة على اساس القاعدة النظريه والعلاقات الحسابيه التي تصف الخواص الصوتيه-البصريه لثلاث مواد مختارة وهي "الزجاج, الجرمانيوم و اوكسيد التريليوم". تم كتابه برنامجين باستعمال لغه "MATLAB", الاول يستعمل لاظهار المعيارية في الشدة لمراتب الحيود كدالة للفاصله الطوريه باستعمال المعادلات التفاضليه الجزئيه, بينما البرنامج الثاني يستعمل لدراسه المعيارية في شدة المجال الكهربائي كدالة لزمن انتقال الموجه وانتقال الموجه الكهرومغناطيسيه باتجاه المحاور الثلاثة بطريقه الفروقات المحددة لمجال الزمن. من خلال النتائج لمادتي الزجاج واوكسيد التريليوم تبين بان التغير الدوري للمعيارية في شدة مراتب الحيود بين المرتبه الصفريه والمرتبه الاولى تصبح صغيرة بزيادة طول التفاعل وهذا يشير الى ان مراتب الحيود الاعلى تبدو واضحه جدا في هذه المواد. النتائج لمادة الزجاج تبين بان المعيارية في شدة المجال الكهربائي تزداد مع انتقال الموجه الكهرومغناطيسيه باتجاه المحاور الثلاثة. النتائج لمادة الجرمانيوم تبين بان التغير بشدة مرتبة الحيود الصفرية تضمحل بسرعة وتتطابق مع مراتب الحيود العالية.

جمهورية العراق

وزارة التعليم العالي والبحث العلمي

جامعه النهرين

كليه العلوم

قسم الفيزياء

محاكاة حاسوبية لجهاز صوتي-بصري لنظام فوتوني

اطروحه مقدمه الى كليه العلوم في جامعه النهرين

كاحد المتطلبات الجزئيه لنيل درجه الماجستير في علوم الفيزياء.

من قبل

مروة كمال مصطفى

بكالوريوس

2008

بأشراف

الاستاذ الدكتور اياد عبد العزيز العاني

الدكتور احمد كمال احمد

2010

1431هـ

CHAPTER FIVE

Conclusions and Suggestions for Future Works

5.1 conclusions:

From the results shown in previous chapters, we can conclude that

1. The results for the Glass material and Tellurium-Oxide material shows that the periodic exchange of intensity between the two main diffracted orders zero and first becomes smaller as the interaction length D increase, this indicate that the higher orders may appear very clear in these materials.
2. The results for Germanium shows that the peak intensity exchange for the zero diffracted order vanish quickly and coincidence with the higher diffracted orders. The results for Tellurium-Oxide material was the best material more than Glass and Germanium materials because it has large values of Q. Moreover, -1 diffracted order may disappear, so that it satisfies the condition of Bragg regime more than other materials.
3. The results for the Glass material shows that the normalized intensity of the electric field increase with the E.M.W. propagation at x, y, and z direction.
4. For Germanium and Tellurium-Oxide crystals the normalized intensity of the electric field decreases with increasing E.M.W. propagation
5. The intensity of the electric field decreases with increasing the E.M.W. propagation this is shown clearly for Tellurium-Oxide and glass materials.

5.2- Suggestion For Future Work

1. Solving the wave equation using Monte Carlo method for the same materials.

2. Construct the acousto-optic modulation device experimentally.

CHAPTER FOUR

Simulation of Strong Interaction Acousto-Optics Waves Using Finite Difference Time Domain

4.1 Introduction

Strong interaction is preferred as a high efficiency mode of operation in acousto-optic devices. Most theories of strong interaction use simplifying assumptions, such as sharply bounded sound columns, which are often realistic [**6**].

In this chapter we use Finite Difference Time Domain method to simulate the strong interaction acousto-optic waves.

A software program has been written using MATLAB software to simulate the distribution of the intensity of the electric field versus propagation of the electromagnetic wave “E.M.W” in a three dimension scale using Finite Difference Time Domain.

4.2 Finite Difference Time Domain

Finite Difference Time Domain “FDTD” is a popular computational electro-dynamics modeling technique. It is considered easy to understand and to implement in software. Since this method using time domain, the solutions can cover a wide frequency range with a single solution run which is called shut solution. Since 1990, FDTD techniques applied in many modeling application ranging from geophysics (involving the entire earth, ion sphere waveguide) Through microwaves (radar signature technology) and antennas (wireless communication devices) [**31**]

During the past 25 years the FDTD method has become the most widely used simulation tool of electro-magnetic phenomena. It has been applied to many problems of propagation, radiation, and scattering of electro-magnetic waves [**32**].

FDTD applied to estimate the path loss in various infrastructure types, tunnels, water distribution networks, and bridges due to its accuracy, flexibility, and potential for visualizing the simulation results. However, problems occur owing to the high memory requirement and heavy computational burden when dealing with these large scale systems using this technique [**33**].

There are five primary reasons for the tremendous expansion of interest in FDTD computational solution approaches for Maxwell's equations these are [**34**]:

1. FDTD uses no linear algebra. Being a fully explicit computation, FDTD avoids the difficulties with linear algebra that limit the size of frequency-domain integral-equation.

2. FDTD is accurate and robust. The sources of error in FDTD calculations are well understood, and can be bounded to permit accurate models for a very large variety of electromagnetic wave interaction problems.
3. FDTD treats nonlinear behavior naturally. Being a time-domain technique, FDTD directly calculates the nonlinear response of an electromagnetic system.
4. FDTD is a systematic approach. With FDTD, specifying a new structure to be modeled is reduced to a problem of mesh generation rather than the potentially complex reformulation of an integral equation. For example, FDTD requires no calculation of structure-dependent Green functions.

5. Computer visualization capabilities are increasing rapidly. While this trend positively influences all numerical techniques, it is of particular advantage to FDTD methods, which generate time-marched arrays of field quantities suitable for use in color videos to illustrate the field dynamics.

In this chapter we adapt three types of crystals these are: Glass "G", Germanium "Ge" and Tellurium-Oxide "Teo_2"

4.3 Results and discussion

The results using FDTD, show the variation of the normalized intensity of the electric field with the time. Also, these results have been demonstrated in 3-dimension, i.e the normalized intensity of the electric field with the electromagnetic wave propagation in x, y, and z direction, respectively. All these results have been studied for three types of materials which are: Glass, Germanium, and Tellurium-Oxide.

The incident electric field is given by an equation [1]:

$$E_{inc(r,t)} = Re[E_{inc(r)} e^{jw_o t}] \qquad 4.1$$

where: $E_{inc}(r,t)$: represent the incident electric field, Re: real part of the incident electric field, w_o : angular frequency of the materials, t : is the propagation time, and j : is the complex number.

Figures (4.1), (4.2), and (4.3) show the behavior of the normalized intensity of the electric field versus time propagation for the Glass, Germanium, and Tellurium-Oxide, respectively.

These figures shows that the normalized intensity decrease with the propagation time in case of Glass and Tellurium-Oxide crystals While, for the Germanium crystal the normalized intensity still constant then very little decreasing with the time propagation, this is due to that the E.M.W. collide with photons so that loss its intensity through its propagation with the space and time, i.e the E.M.W. collides with photons in Glass and Tellurium-Oxide more than Germanium.

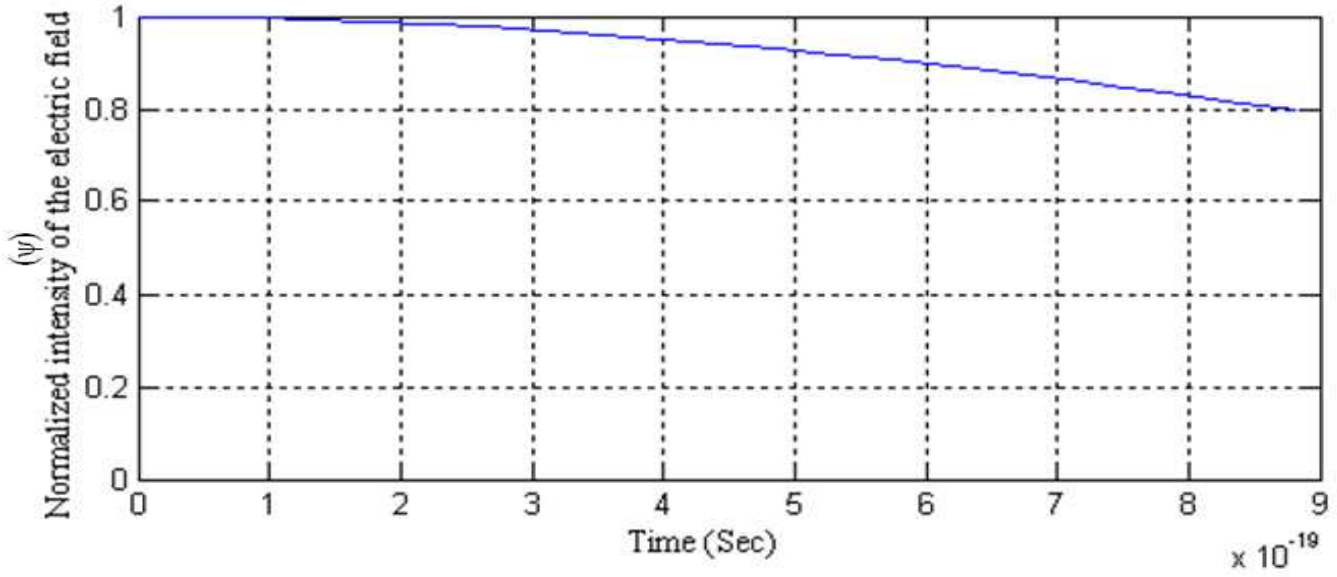

Figure (4.1): Normalized intensity of the electric field versus time propagation for Glass crystal

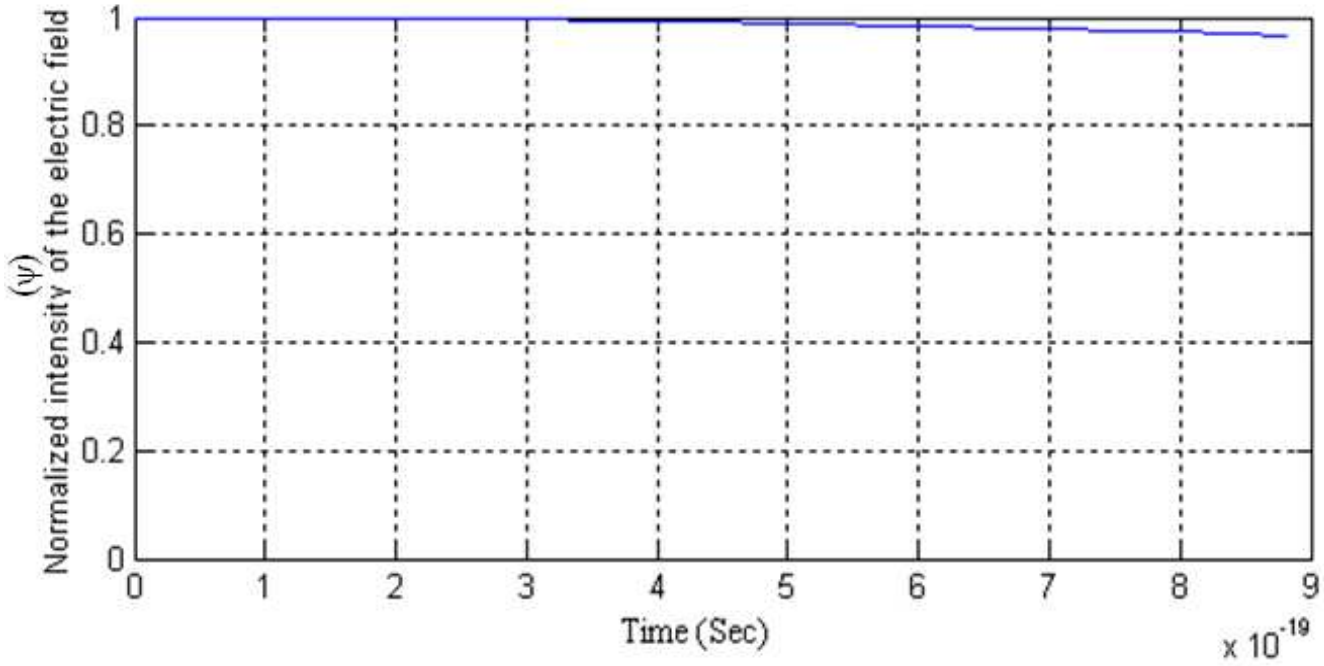

Figure (4.2): Normalized intensity of the electric field versus time propagation for Germanium crystal

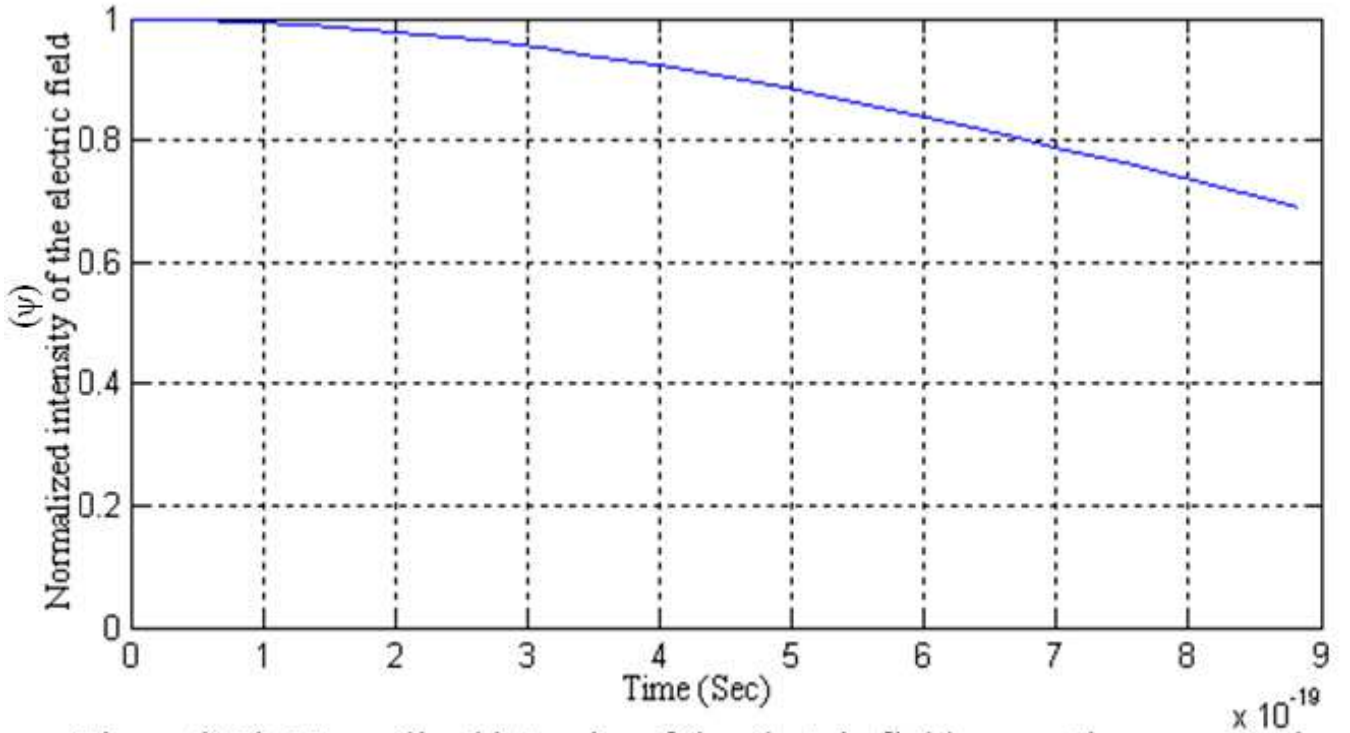

Figure (4.3): Normalized intensity of the electric field versus time propagation for Tellrium-Oxide crystal

Figures (4.4), (4.5), and (4.6) shows the behavior of the normalized intensity of the electric field with electromagnetic wave propagation in x, y, and z directions, respectively for the Glass crystal.

These figures shows that the normalized intensity of the electric field increase with the electromagnetic wave propagation in x, y and z directions from the zero point and the decreasing.

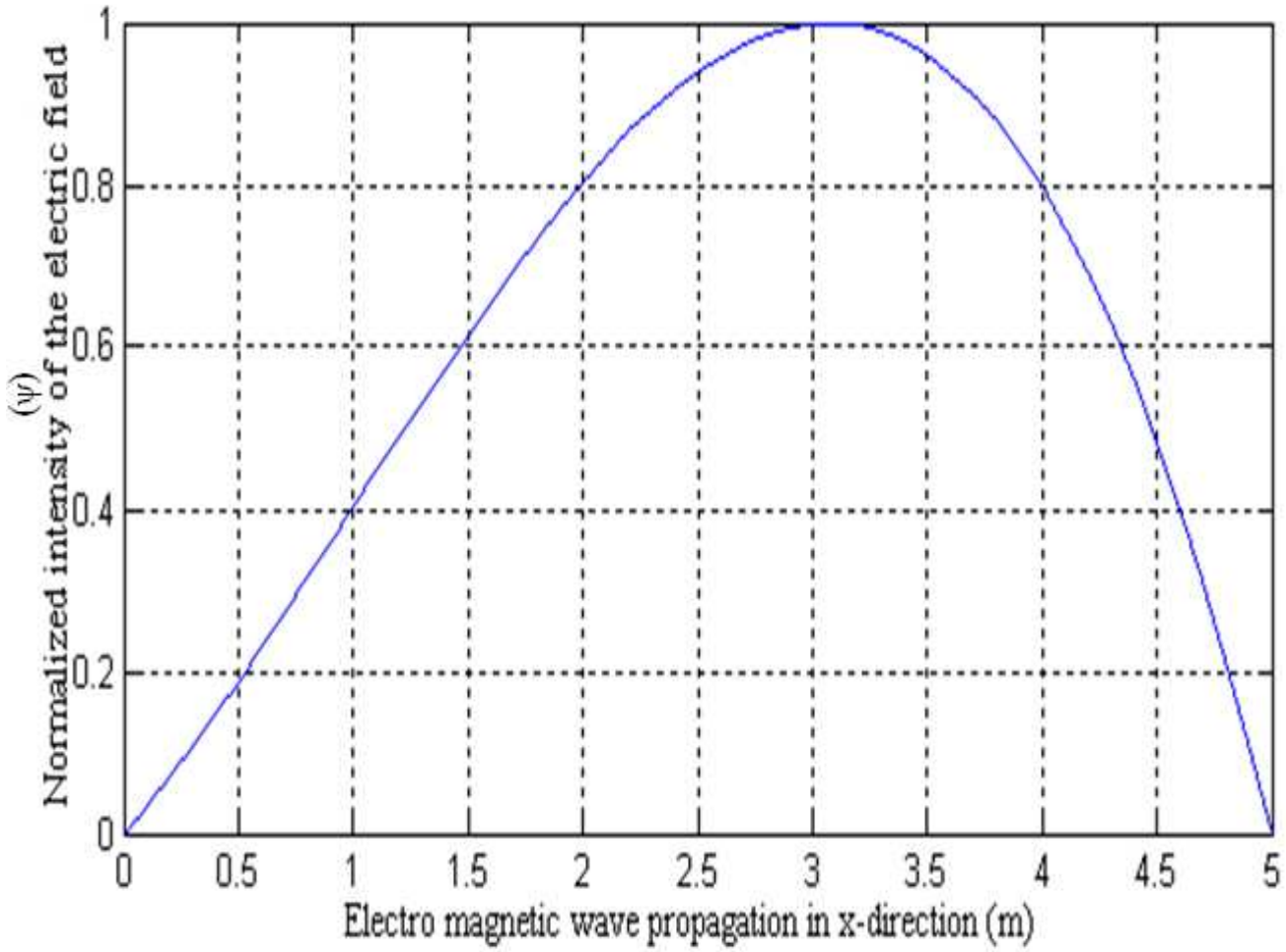

Figure (4.4): Normalized intensity of the electric field versus electro magnetic wave propagation in x-direction for Glass crystal

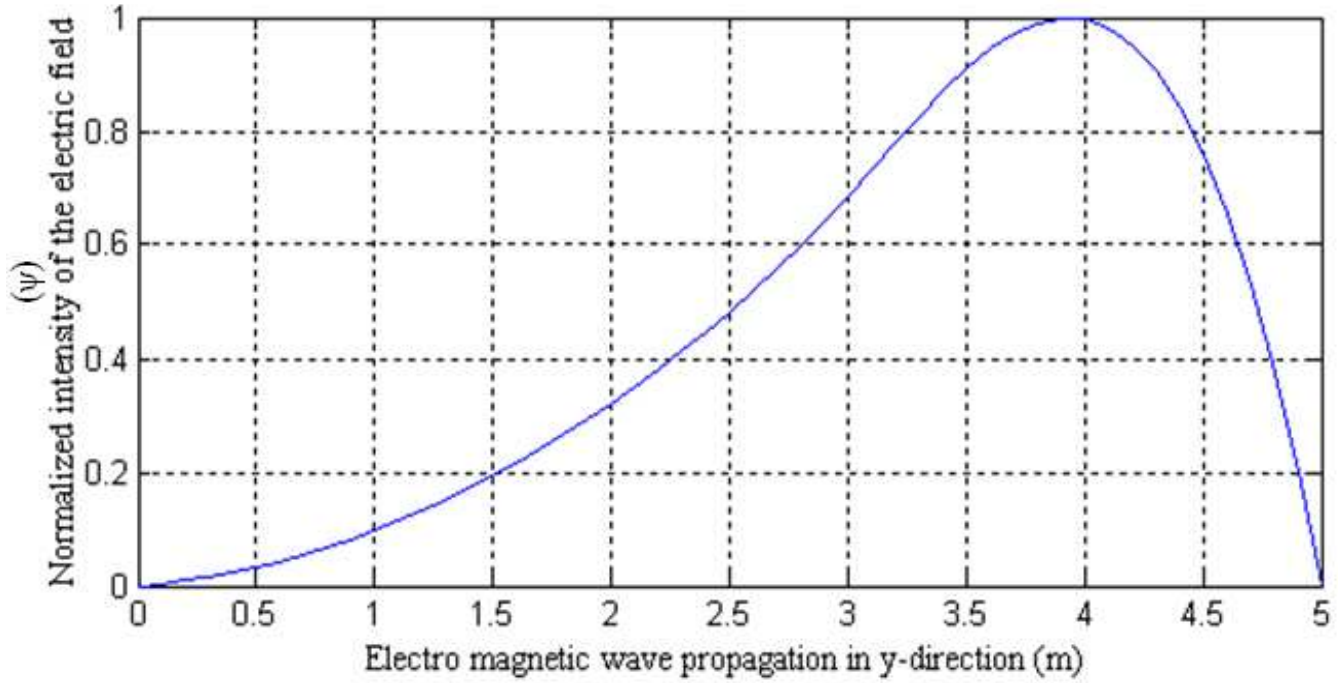

Figure (4.5): Normalized intensity of the electric field versus electro magnetic wave propagation in y-direction for Glass crystal

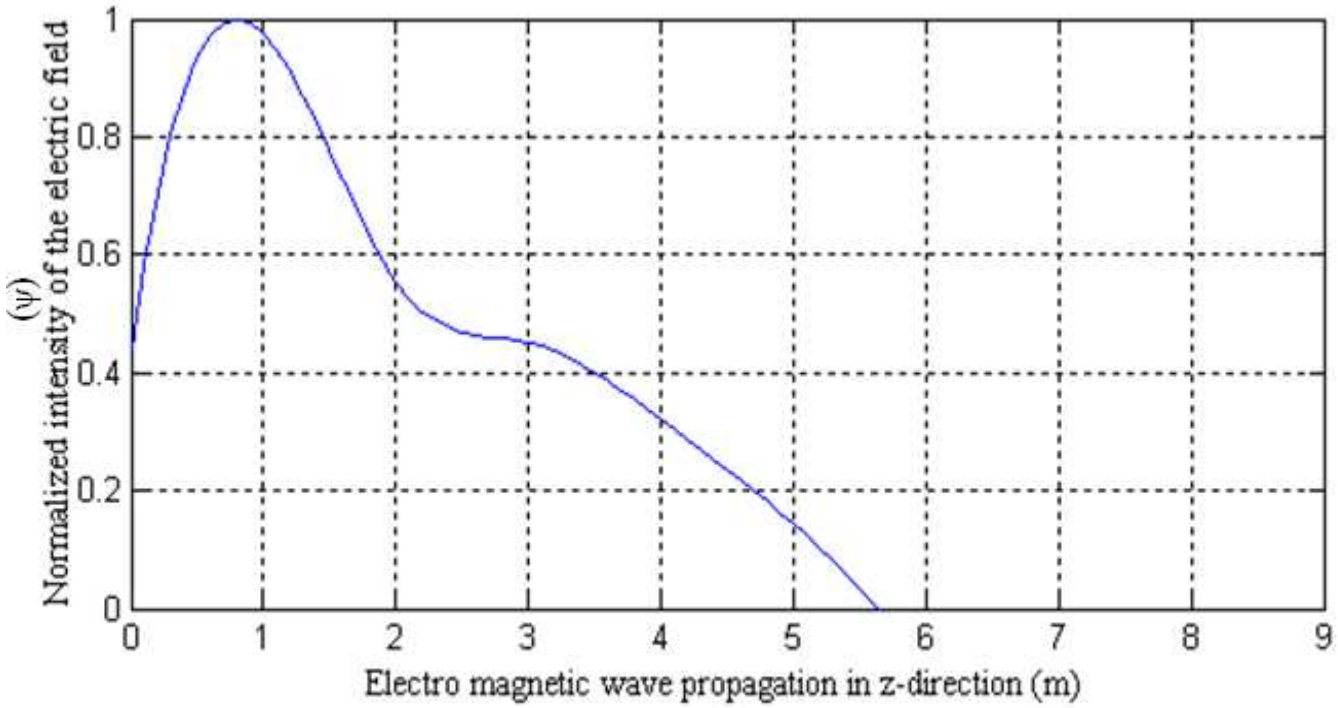

Figure (4.6): Normalized intensity of the electric field versus electro magnetic wave propagation in z-direction for Glass crystal

Figures (4.7), (4.8), and (4.9) shows the behavior of the normalized intensity of the electric field versus electro-magnetic wave propagation in x, y, and z directions, respectively for Germanium crystal.

All These figures have been demonstrated that the normalized intensity has similar trend in x and y directions with Glass crystal while, in the z direction the normalized intensity decrease without increasing.

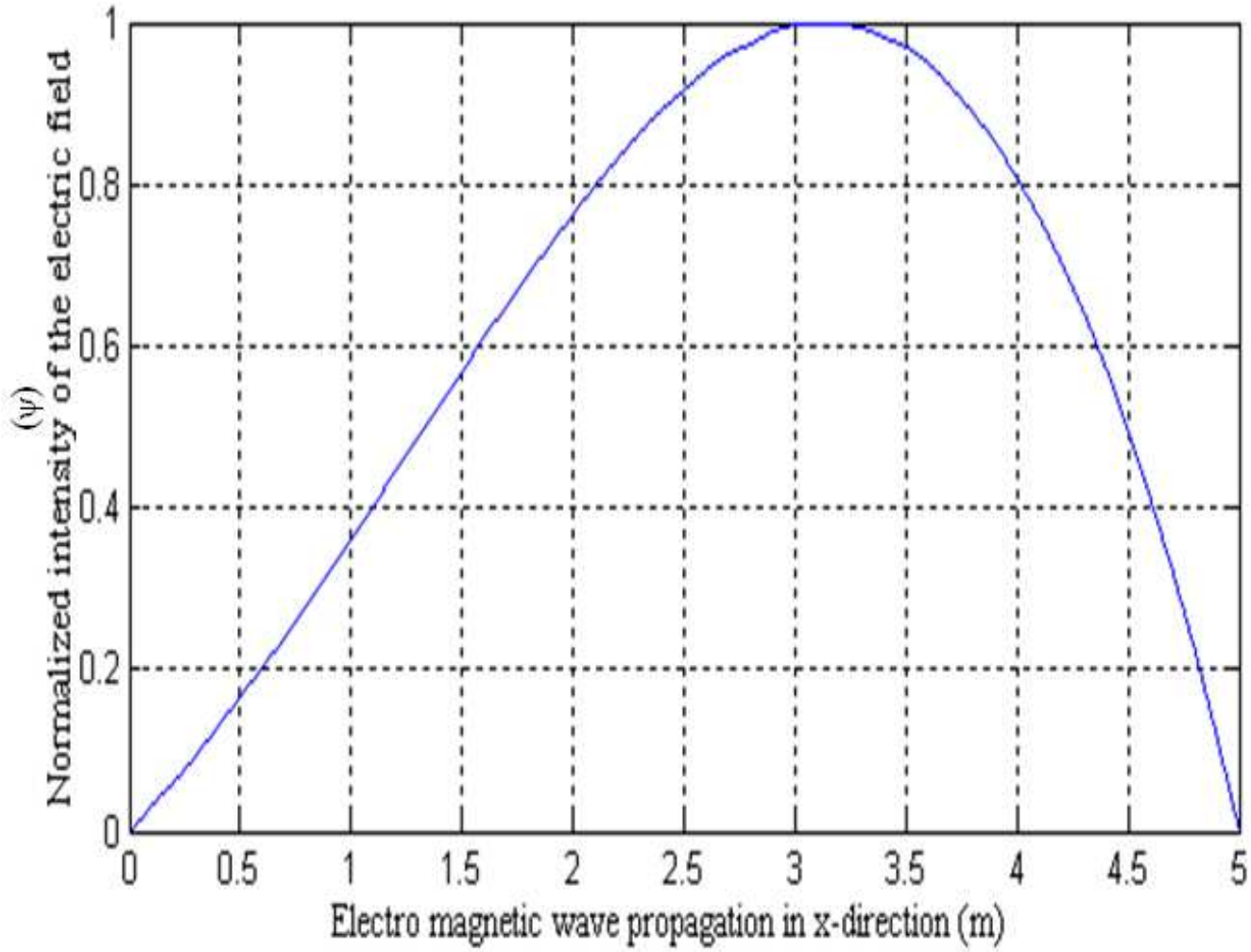

Figure (4.7): Normalized intensity of the electric field versus electro magnetic wave propagation in x-direction for Germanium crystal

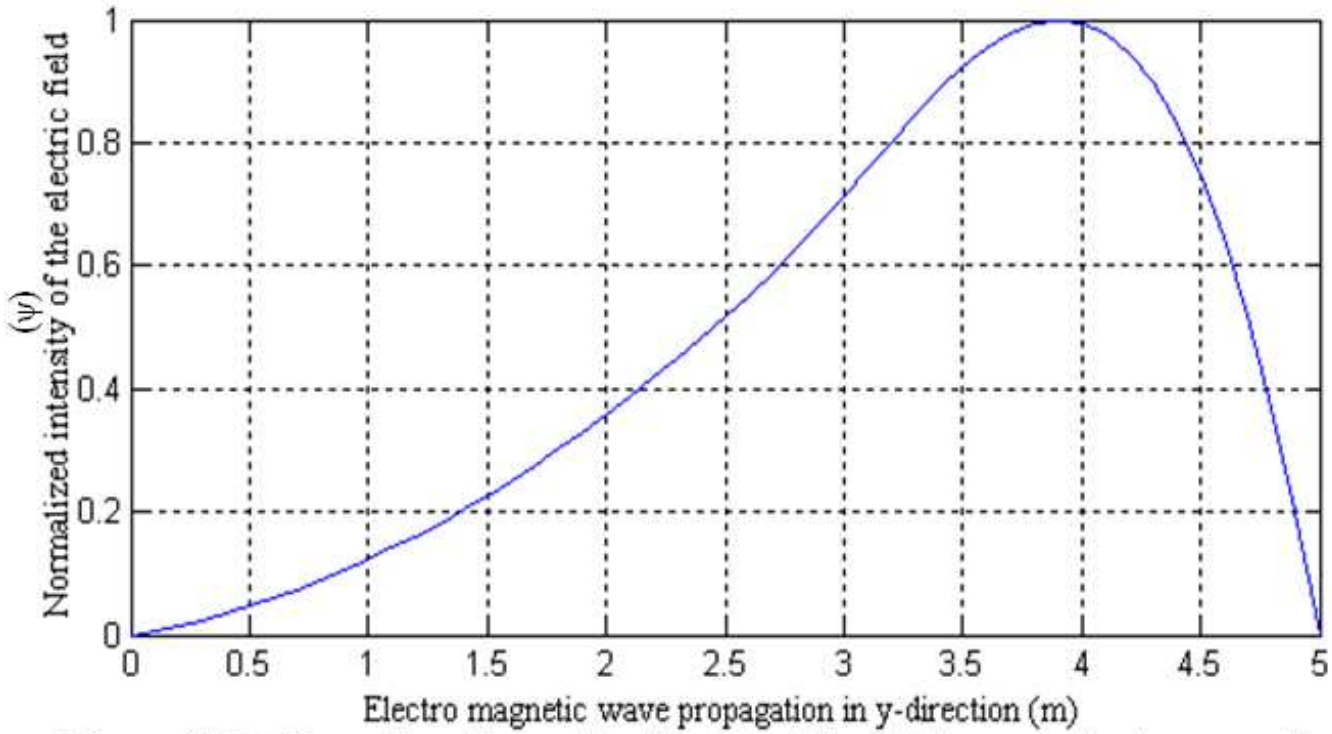

Figure (4.8): Normalized intensity of the electric field versus electro magnetic wave propagation in y-direction for Germanium crystal

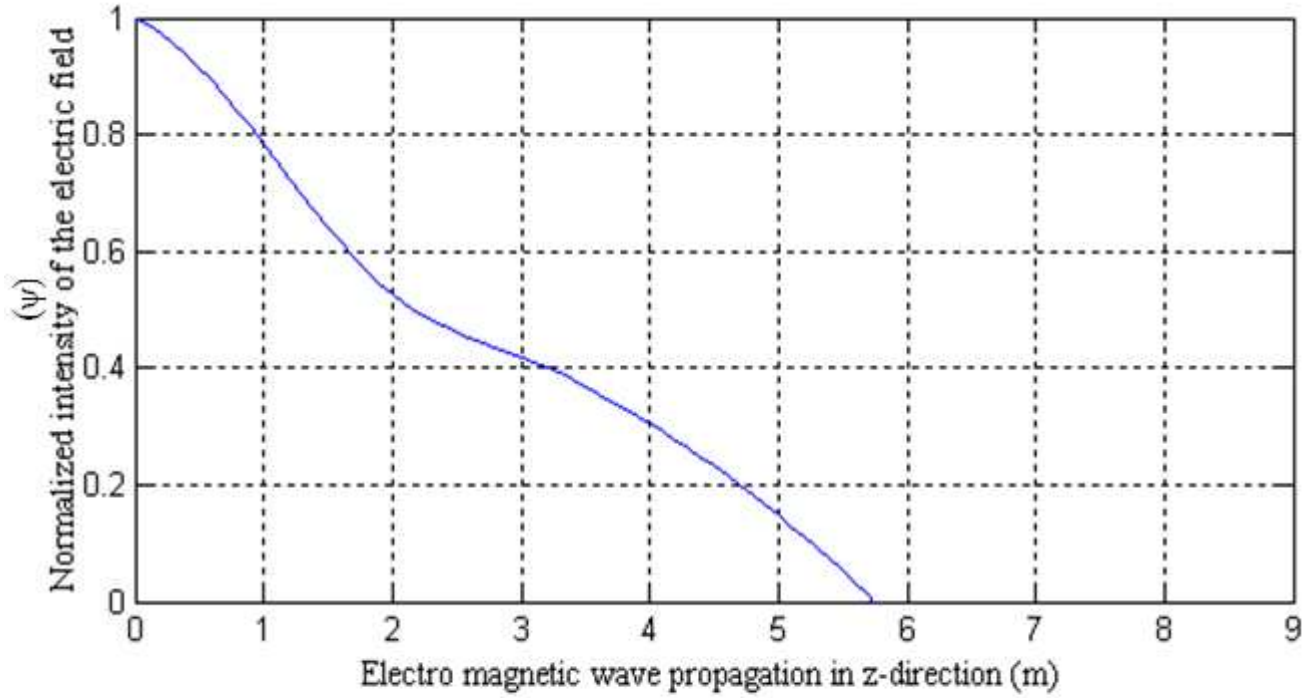

Figure (4.9): Normalized intensity of the electric field versus electro magnetic wave propagation in z-direction for Germanium crystal

Figures (4.10), (4.11), and (4.12) shows the behavior of the normalized intensity of the electric field versus electromagnetic wave propagation in x, y and z directions, respectively for Tellurium-Oxide crystal.

These figures show that the normalized intensity has similar trend in x and y directions (same behavior of Glass and Germanium) crystals while, in the z direction the normalized intensity increase and then decrease that is different behavior about the z direction for the Germanium crystal.

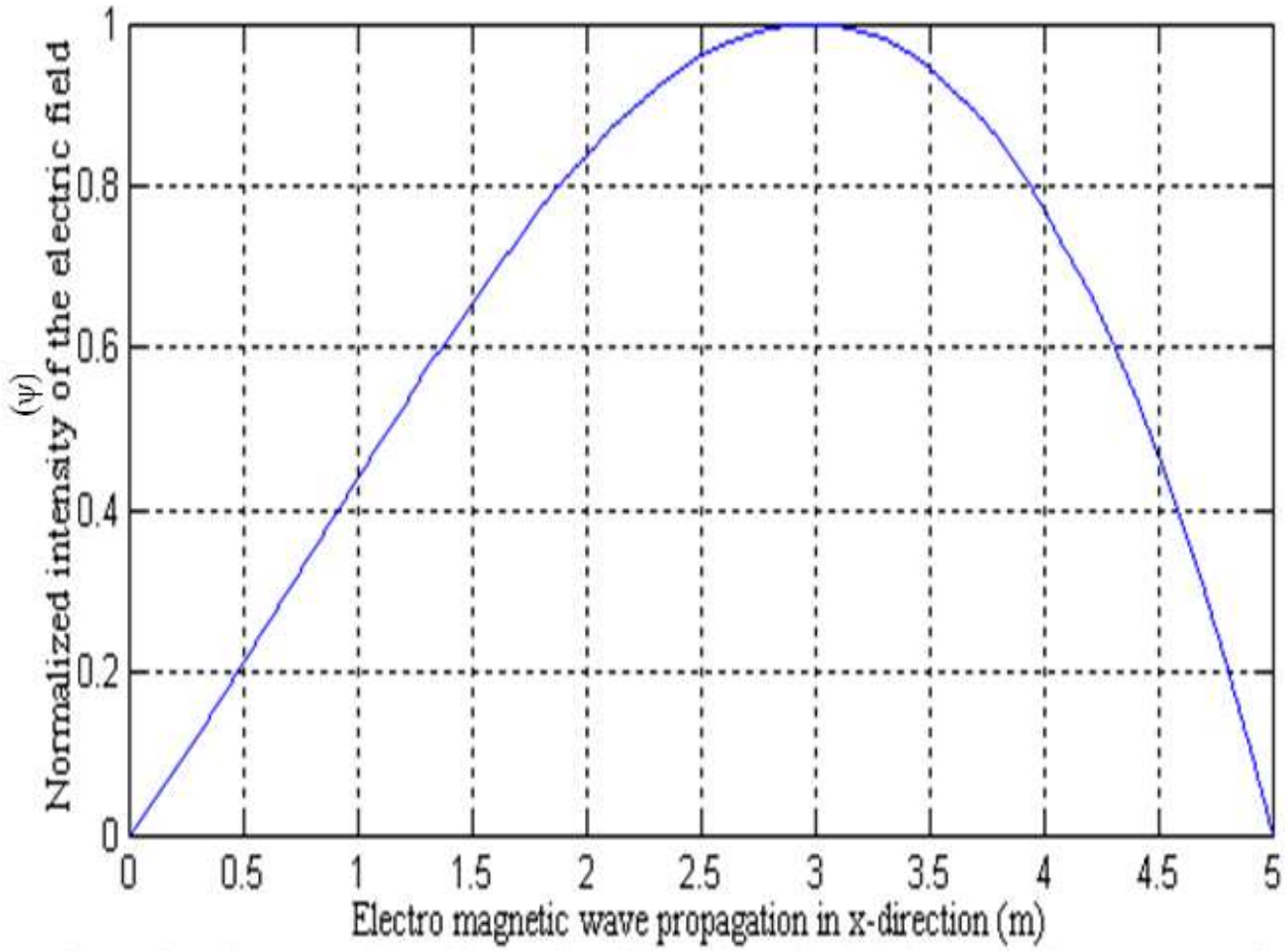

Figure (4.10): Normalized intensity of the electric field versus electro magnetic wave propagation in x-direction for Tellrium-Oxide crystal

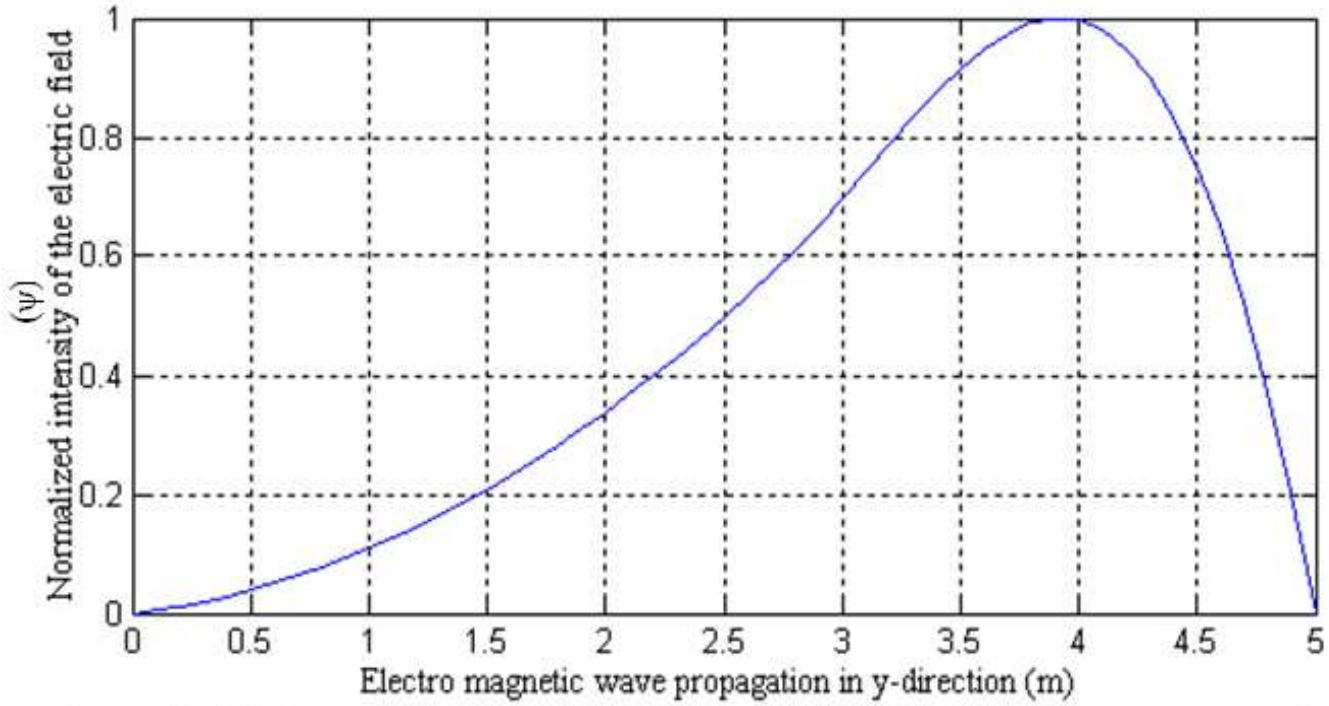

Figure (4.11): Normalized intensity of the electric field versus electro magnetic wave propagation in y-direction for Tellrium-Oxide crystal

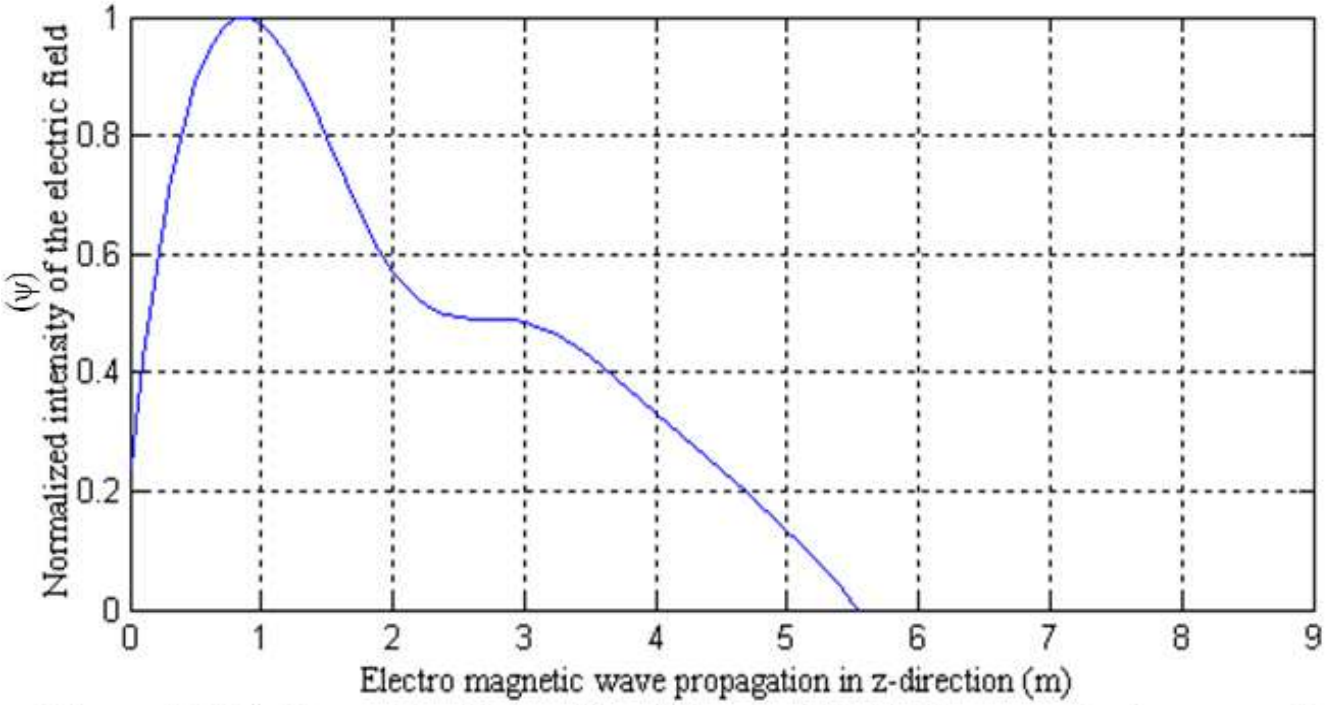

Figure (4.12): Normalized intensity of the electric field versus electro magnetic wave propagation in z-direction for Tellrium-Oxide crystal

Figures (4.13) and (4.14) show the behavior of the normalized intensity of the electric field versus electromagnetic wave propagation in 3-dimention scale and its contour, respectively for Glass crystal. Moreover, these figures show that the normalized intensity of the electric field in z direction reaches to the maximum value than the Germanium, and Tellurium-Oxide crystals.

While, figures (4.15) and (4.16) show the behavior of the normalized intensity of the electric field versus electromagnetic wave propagation in 3-dimention scale and its contour, respectively for Germanium crystal. These figures show that the normalized intensity at the z direction has a value less than the Glass crystal.

Then, figures (4.17) and (4.18) show the behavior of the normalized intensity of the electric field versus electromagnetic wave's propagation in 3-dimention scale and its contour, respectively for Tellurium-Oxide crystal. These figures show that the normalized intensity has little increasing than the Germanium crystal.

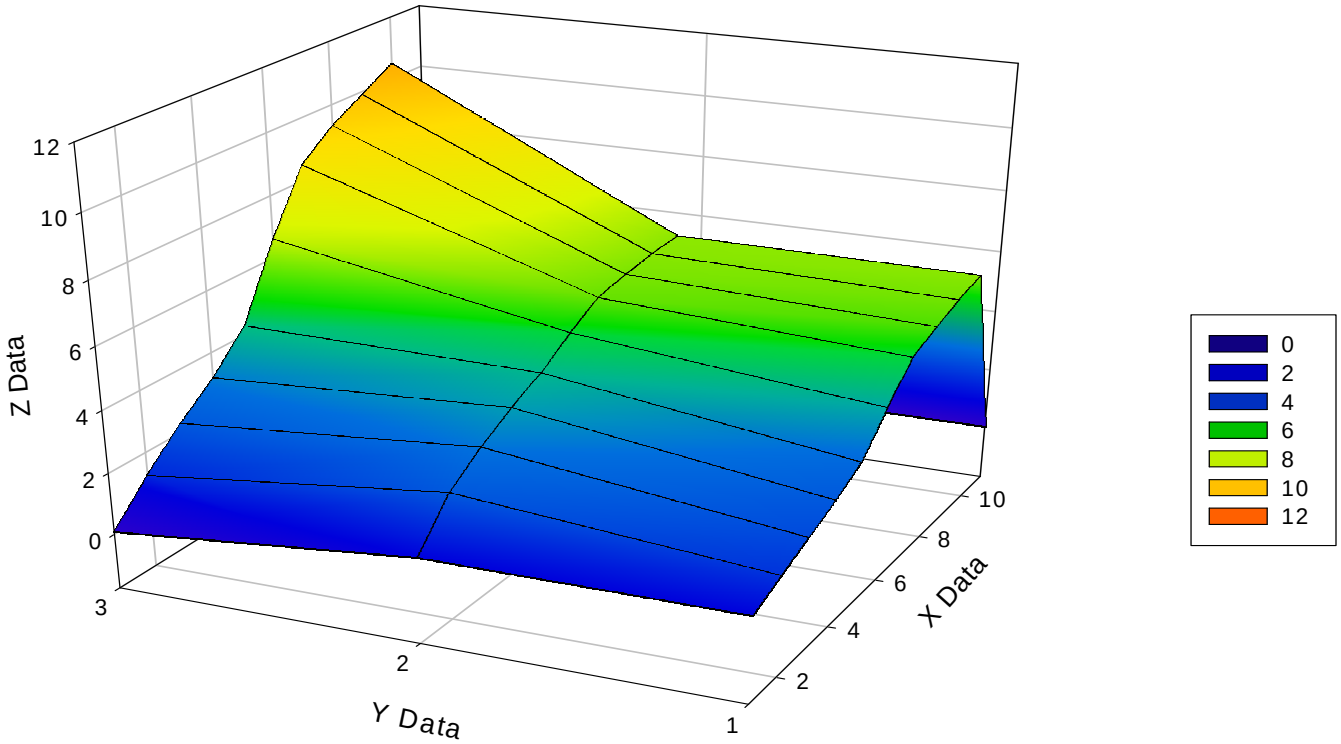

Figure (4.13): 3-D Normalized intensity variation of the electric field versus electro magnetic wave propagation for glass crystal

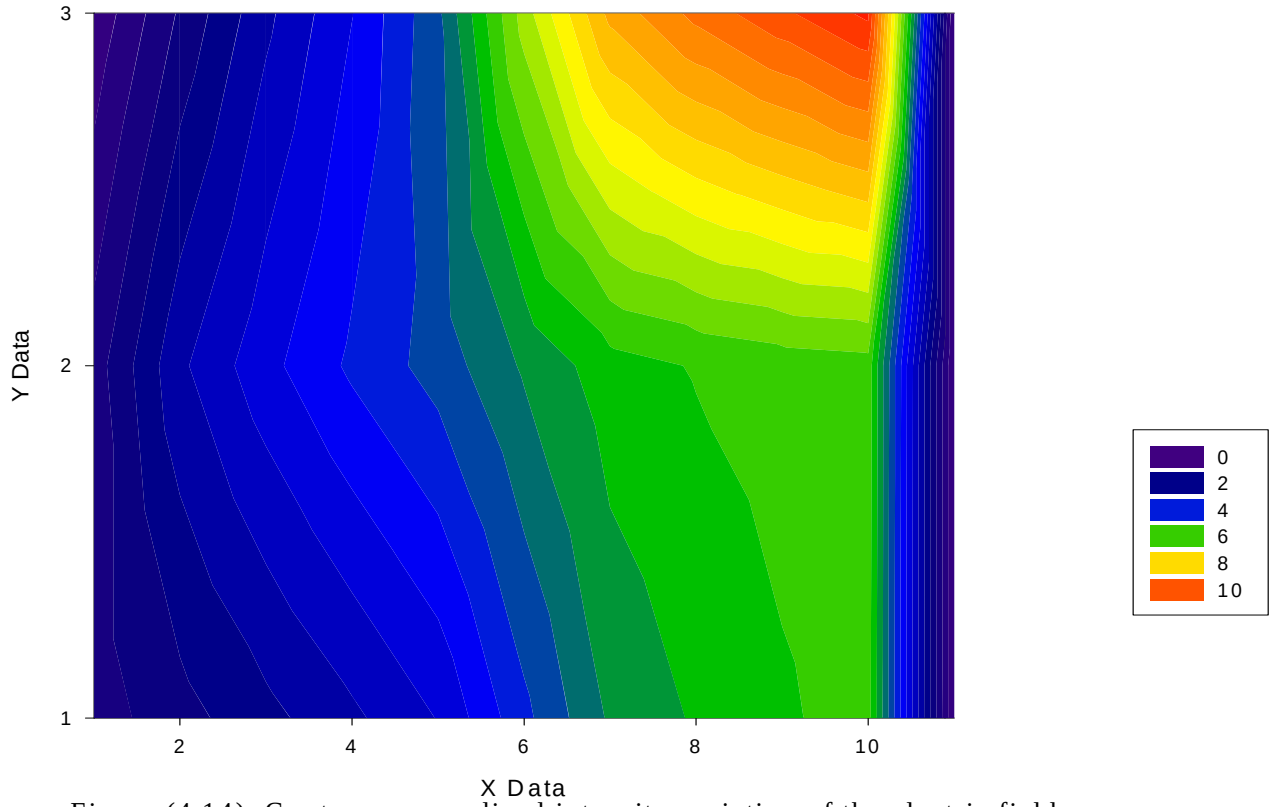

Figure (4.14): Contoure normalized intensity variation of the electric field versus electro magnetic wave propagation for glass crystal

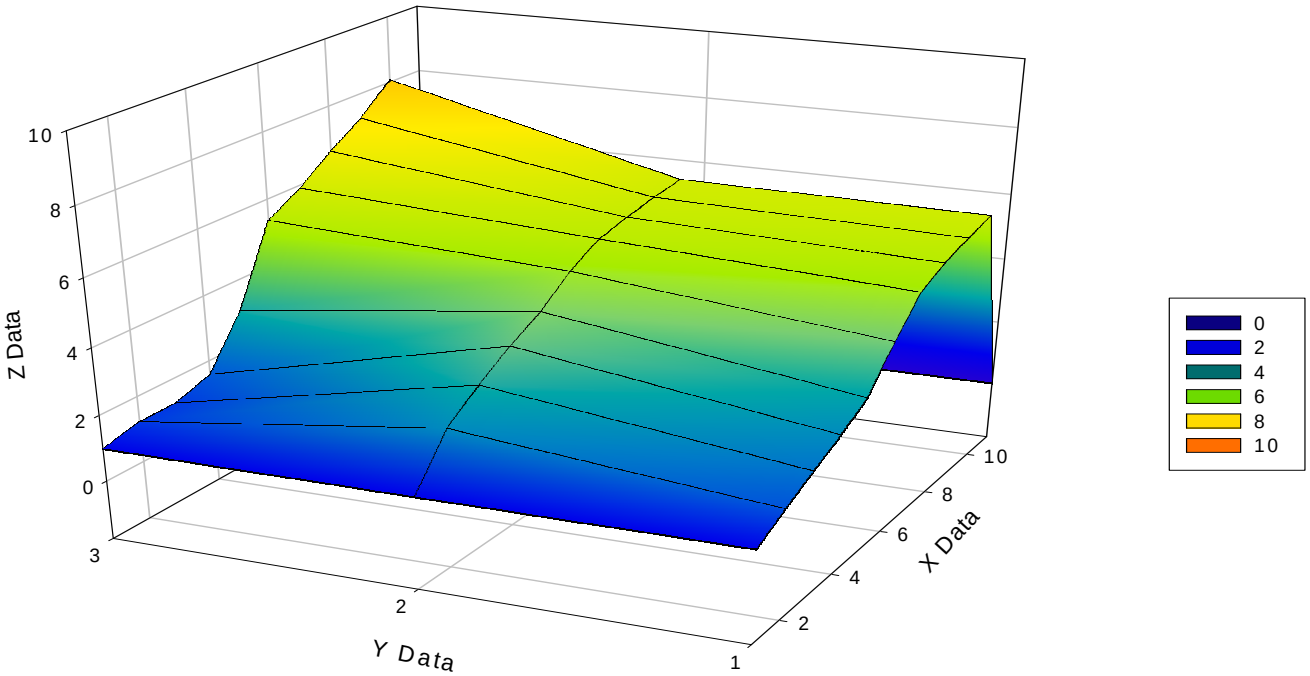

Figure (4.15): 3-D normalized intensity variation of the electric field versus electro magnetic wave propagation for Germanium crystal

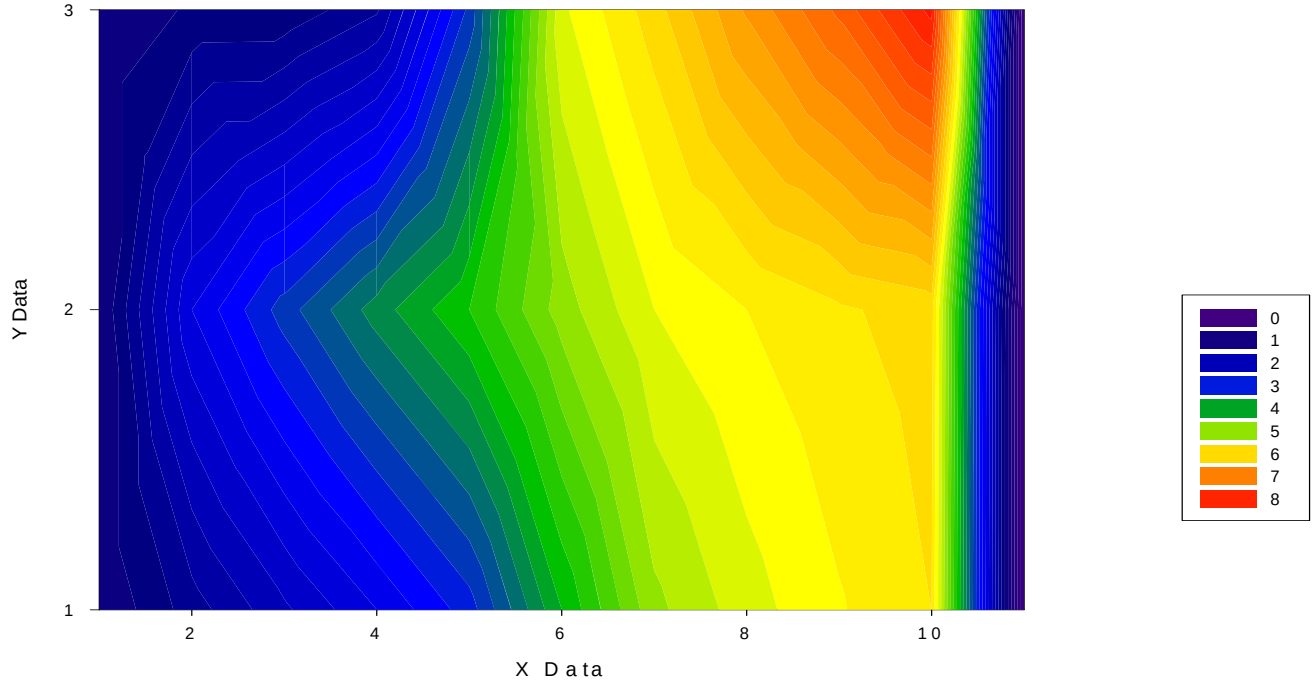

Figure (4.16): Contoure normalized intensity of the electro magnetic field versus electro magnetic wave propagation for Germanium crystal

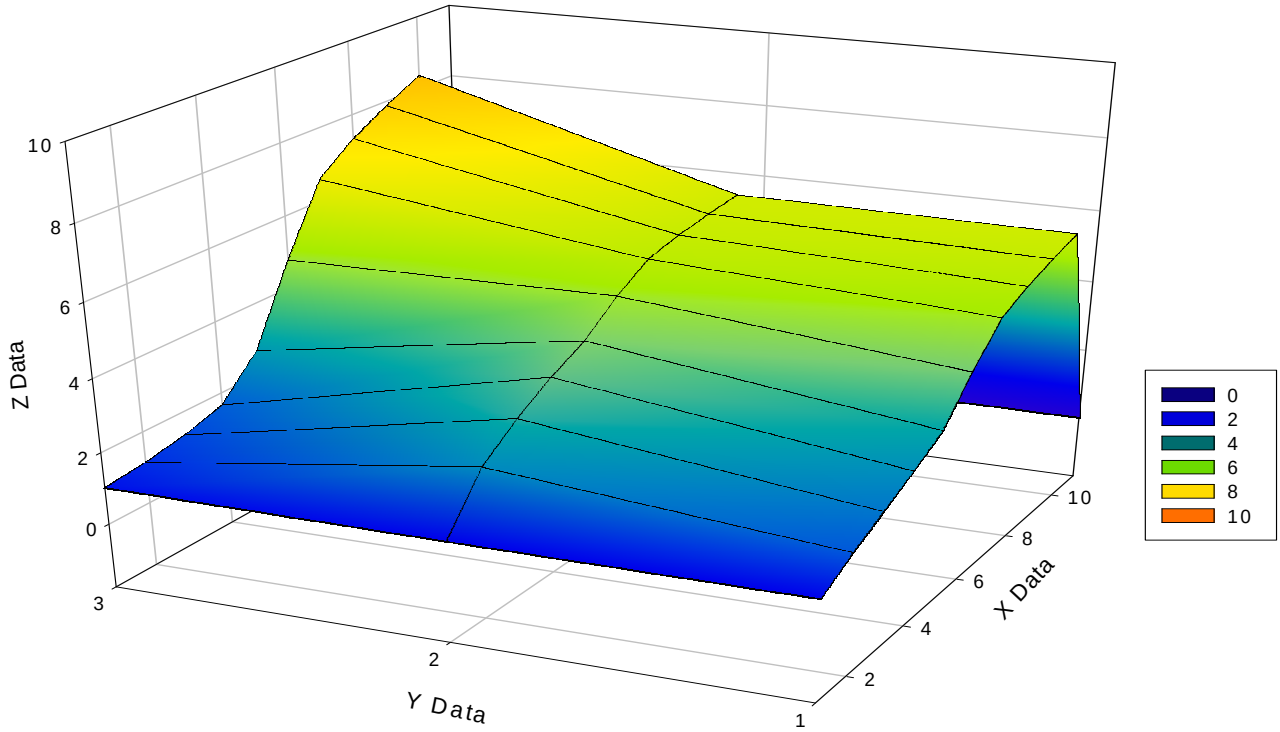

Figure (4.17): 3-D normalized intensity variation of the electric field versus electro magnetic wave propagation for Tellrium-Oxide crystal

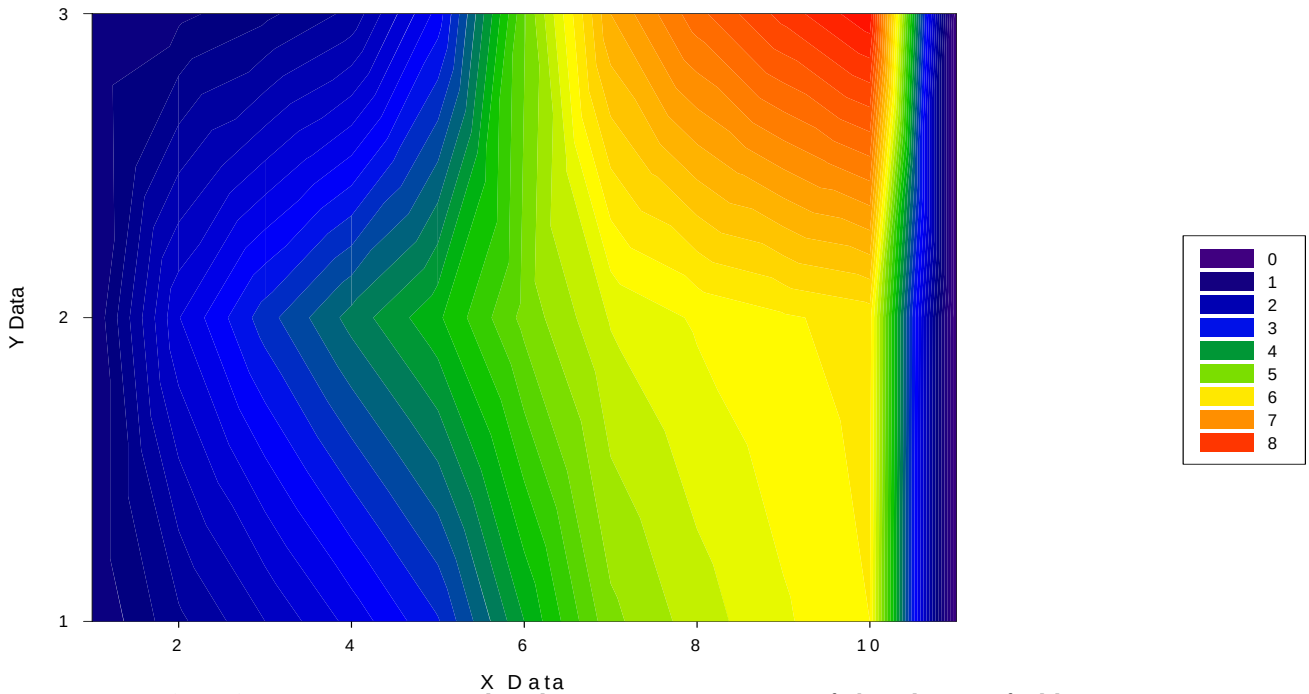

Figure (4.18): Contoure normalized intensity variation of the electric field versus electro magnetic wave propagation for Tellrium-Oxide crystal

4.4 Conclusions:

The results for the Glass material show that the normalized intensity of the electric field increases with the E.M.W. propagation. While, for Germanium and Tellurium-Oxide crystals the normalized intensity of the electric field decreases with increasing E.M.W. propagation.

CHAPTER ONE

Introduction of Acousto-Optics

1.1 General Introduction

Acousto-optics science "AO" deals with the interaction between sound and light waves. As a result of acousto-optic interaction, the electrical signal modulates the light waves. The piezoelectric transducer converting the electrical signal into the sound waves propagating in the acoustic medium. The rarefaction and compression waves, which are created by the pressure in the sound waves, causes the perturbation of the refractive index. The incident light splits into various diffracted orders by the phase grating. The directions of the diffracted or scattered light inside the sound cell which are given by **[1]:**

$$\sin \phi_m = \sin \phi_{inc} + m \lambda_0 / \Lambda \qquad 1.1$$

Equation (1.1) is known as equation of grating.

Where: m is the diffraction order, ϕ_{inc} is the angle of incident light, ϕ_m is the angle of the m^{th} order of diffracted light, λ_0 is the wavelength of the incident light, and Λ is the acoustic wavelength.

Fig. (1.1) shows the schematic diagram of acousto-optic modulator [**1**].

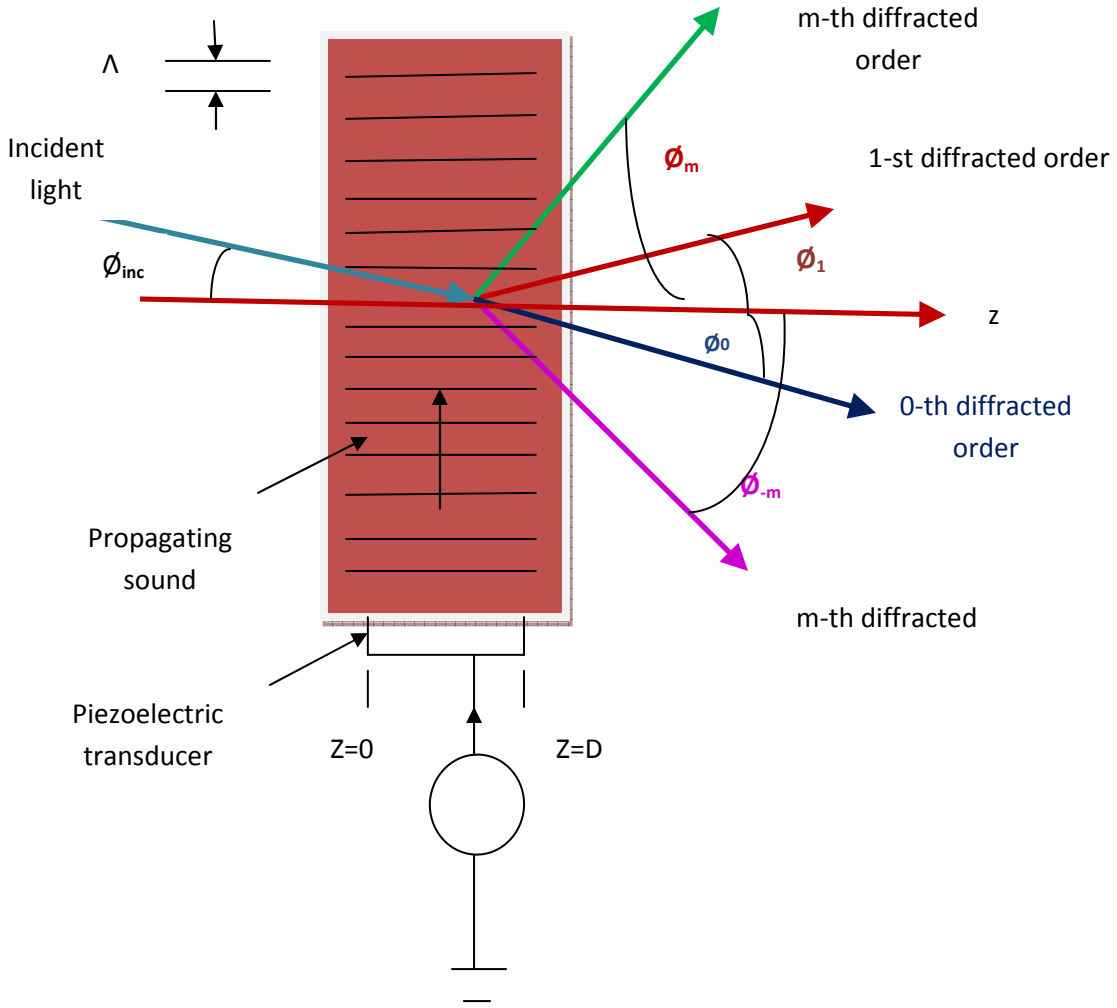

Figure (1.1): Acousto-optic modulator [**1**].

Figures (1.2) and (1.3) shows the up shifted and down shifted interactions, respectively, where (a) represents the wave vector diagram and (b) represents the experimental configuration [**1**].

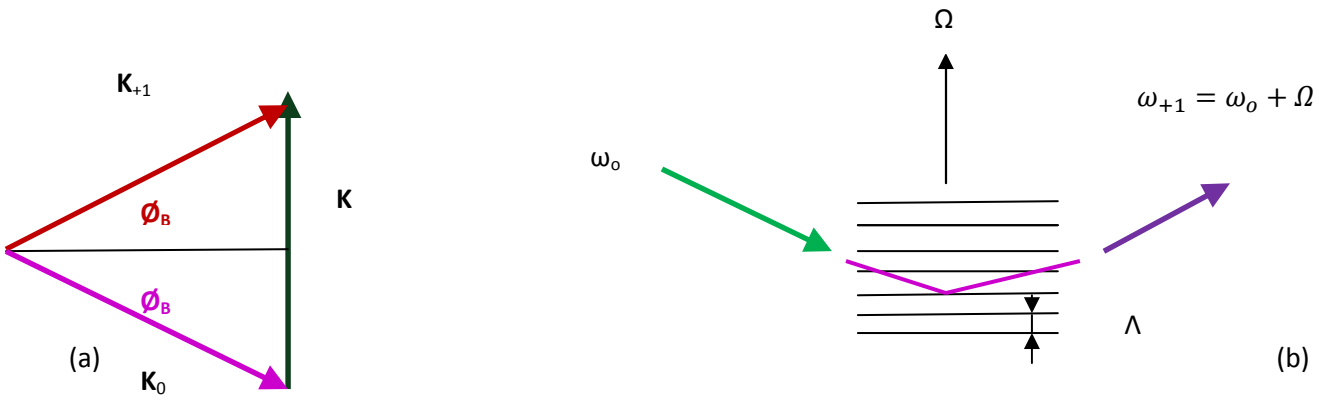

Figure (1.2) shows the up-shifted frequency of the sound interaction: a wave-vector diagram; b- Experimental configuration [**1**].

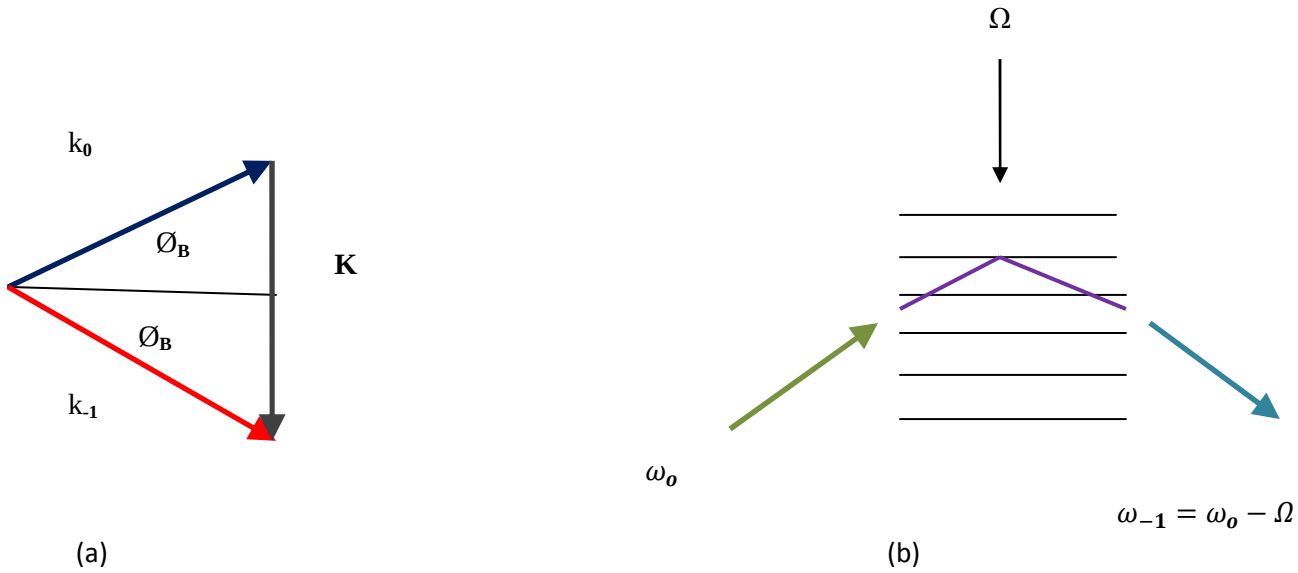

Figure (1.3): The down-shifted frequency of the sound interaction: a- Wave-vector diagram; b- Experimental configuration [**1**].

Up-shifted interaction can be represented by the following equations [**1**]

$$k_{+1} = k_0 + k \quad 1.2$$

$$w_{+1} = w_0 + \Omega \quad 1.3$$

while, the down-shifted interaction can be represented by the following equations [**1**]

$$k_{-1} = k_0 - k \quad 1.4$$

$$w_{-1} = w_0 - \Omega \quad 1.5$$

where k_0 represents wave vector of the light incident plane and k_{+1} represent wave vector of diffracted (or scattered) plane wave of light. w_0, Ω, and w_{+1} are the angular frequencies of the incident light, sound wave, and scattered light, respectively.

1.2 Surface Acoustic Waves

Guided optical waves in waveguides (either planar or strip guides) are tightly confined to a region close to the substrate surface. To achieve an efficient interaction between the guided optical waves and the acoustic wave, the acoustic field should be localized in this region. Small part of acoustic wave may interact with the optical wave since these waves extend over the substrate volume. Rayleigh in 1888 predicted that the surface acoustical wave is a solution of the acoustical wave equation. Nowadays, Surface Acoustic Waves "SAW" find a wide rang of applications, in particular, in radio frequency RF-electronics, where SAW devices are used for signal processing and frequency filtering.

In most materials, SAW have a complex structure. They are neither longitudinal nor transverse waves. The amplitude and the direction of the mechanical displacement of a point in a crystal are strongly dependent on the distance from the substrate surface [**2**].

1.3 Planer Waveguide Type Acousto-Optical Deflectors

Bragg type Acousto-Optical Deflectors "AOD" and Acousto-Optic Modulators "AOM" are well established optic components with a variety of application. Therefore, it was obvious to develop equivalent integrated optical circuits.

The basic structure of an acousto-optical Bragg deflector in a planer waveguide can be shown in figure (1.4) [**2**].

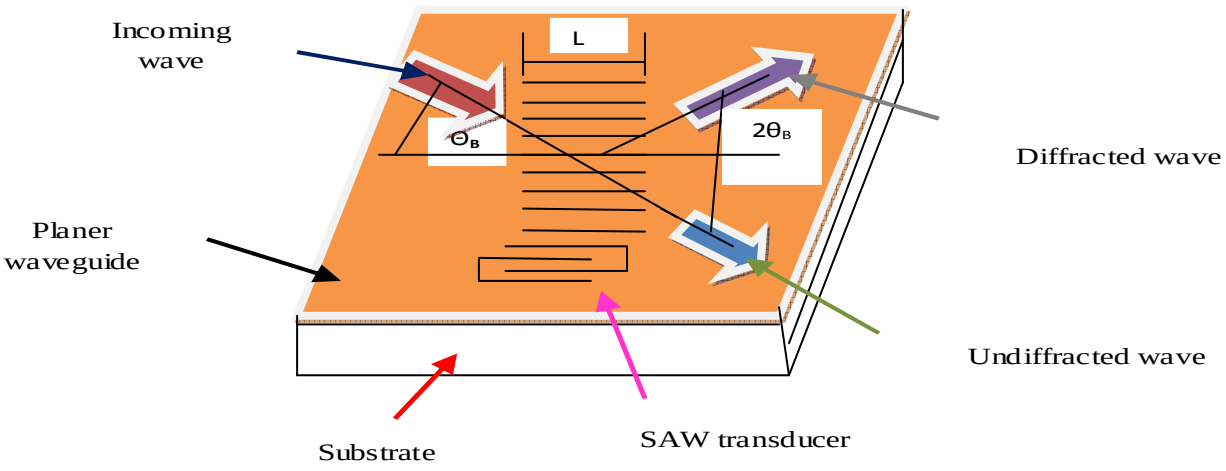

Figure (1.4): The basic structure of an integrated acousto-optical Bragg deflector in a planer waveguide [**2**]

The efficient interaction between acoustic waves with the guided optical wave occurs when the SAW is excited on the substrate surface. The Klein-Cook parameter "Q" is defined as [**2**]:

$$Q = \frac{2\lambda\pi d}{n\Lambda^2} \qquad 1.6$$

where d is the interaction length of material and n is the refractive index of materials, Q<<1 leds to Raman-Nath regime. while, Q>>1, leds to Bragg regime.

The frequency of the diffracted light is either up shifted or down shifted from that of the incident light by the frequency of the SAW. The up shifted or down shifted corresponds, respectively, to the case in which the incident wave vector is at an angle larger or smaller than 90^0 from the SAW wave vector. The diffraction efficiency is proportional to $\sqrt{P_a}$, where P_a is the power of the acoustic wave [**2**].

1.4 Acousto-Optic Modulators and Deflectors

Acousto-optic component are usually used in laser equipment for electronic control of the modulation and or deflection of the laser beam. The acoustic wave generates a refractive index, which acts a sinusoidal grating in the optical material when the interaction of acoustic waves and light occur in optical materials. The first order beam can be made to have the highest efficiency by [**3**]:

1. A suitable design of the modulator or deflector.

2. The tuning of the incident angle between the laser light and the axis of acoustic propagation in the optical material.

The angle of diffraction "θ" can be written by the following equation [**3**]:

$$\theta = \frac{\lambda f_a}{V_a} = 2\theta_b \qquad 1.7$$

where: f_a is the acoustic frequency, v_a is the acoustic velocity, and θ_b is the Bragg angle.

The diffraction of a light beam by travelling acoustic plane wave in an acousto-optic modulator can be shown in figure (1.5) [**4**].

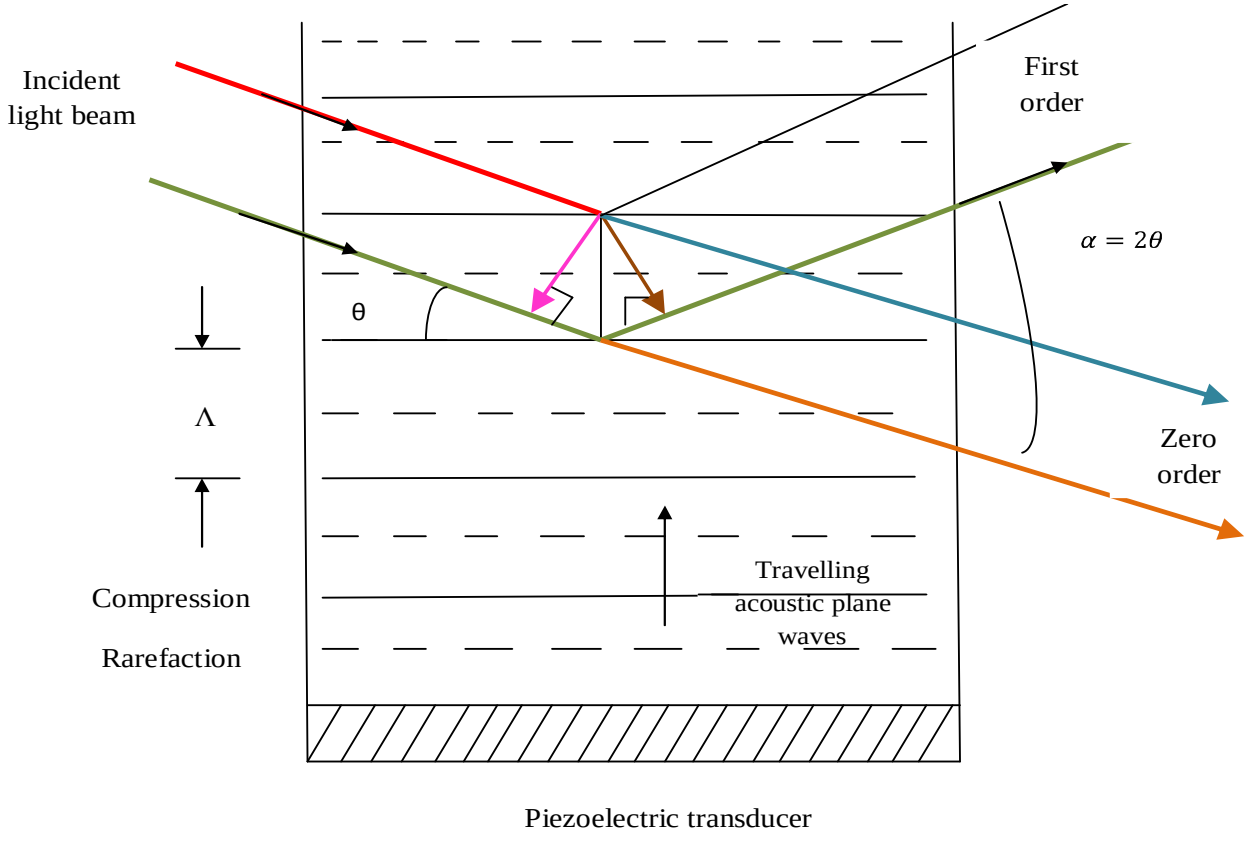

Figure (1.5): The diffraction of a light beam by travelling acoustic plane Wave in an acousto-optic modulator [**4**]

1.5 Acousto-Optic Material Selection

Variety materials are used for acousto-optic modulators depending on the wave, power density, and polarization [**3**]. Table (1.1) illustrates the properties for most common materials used for acousto-optical modulator [**3**].

Table (1.1): Summary of the properties and figure of merit for most common materials used for acousto-optical modulators [**3**].

Material	Optical range Microns	Optical polarization	Refractive . index	Acoustic mode velocity		FIG.of MERIT
AMTIR	1.06-5	Random	2.6	L	$2.6*10^3$	140
Flint Glass SF6	0.45-2	Random	1.8	L	$3.51*10^3$	8
Flint Glass SF10	0.45-2	Random	1.7	L	$4.0*10^3$	5
Fused Silica	0.2-4.5	Linear	1.46	L	$5.96*10^3$	1.5
Fused Silica	0.2-4.5	Random	1.46	S	$3.76*10^3$	0.46
Crystal Quartz	0.2-4.5	Random or Linear	1.55	L	$5.75*10^3$	1.5/2.2
Gallium Phosphate	0.63-10	Linear	3.3	L	$6.65*10^3$	29
Gallium Phosphate	0.63-10	Random	303	S	$4.13*10^3$	17
Germanium	2.0-10	Linear	4	L	$5.5*10^3$	180
Lithium Niobate	0.6-4.5	Linear	2.2	L	$6.6*10^3$	7
Lithium Niobate	0.6-4.4	Linear	2.2	S	$3.6*10^3$	15
Tellurium Oxide	0.4-5	Random	2.25	L	$4.26*10^3$	34
Tellurium Oxide	0.4-5	Circular	2.25	S	$0.62*10^3$	750

Table (1.1) shows the Germanium material is the most common material that used in the application of the acousto-optic modulator with a relative high figure of merit at infrared region. While for fused silica, crystal quartz, and Tellurium Dioxide, we used visible region [**3**].

1.6 Literature Review

Brillouin in 1922 [**5**] predicted only (+1) and (-1) orders of diffraction for a sinusoidal sound wave. The most important theory of acousto-optic modulator was developed in "1930", where the ultrasonic light diffraction phenomenon was developed by Raman and Nagendra [**5**]. Their first approximated theory has assumed a thin column of ultrasonic as a phase grating in which a curvature of light rays could be neglected.

Lucas and Biquard in 1932 [**5**], performed two independent experiments which originated investigations on the ultrasonic and light interaction initiating the new branch of science and applications widely developed as acousto-optics. Recently, the results of these experiments illustrating the diffraction of light by such high-frequency sound waves in a liquid.

Debye and sears in 1932 [**5**], discussing their results has stated that in their experimental conditions the Bragg reflection angle was not sharply if $\frac{L}{\Lambda}$ large compared to $\frac{\Lambda}{\lambda}$ does a sharp where L: is the interaction length, Λ: is the wave length of sound, and λ: is the wave length of light.

In fact a good prediction of acousto-optics Bragg diffraction confirmed experimentally by Bhagavantam and Rao in 1948 [**5**].

Many investigations were carried out to study the nature of the ultrasonic light diffraction in some special configurations in particular in the case of two parallel ultrasonic beams. The theoretical results elaborated by Leroy in 1973 [**5**].

In 1979 [**6**] showed that the Strong interaction is the general case of up shifted Bragg diffraction. The interaction diagram illustrating detailed dynamics in the interaction region are shown in figure [1.6]

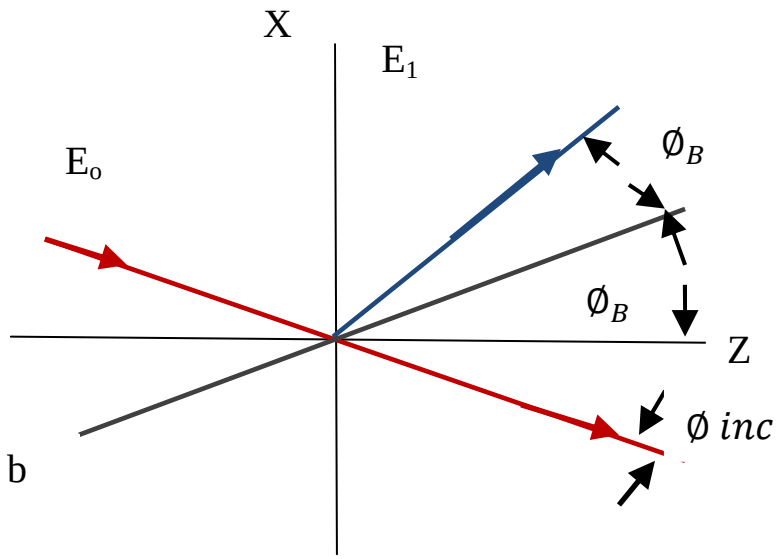

Figure (1.6): shows the interaction diagram illustrating detailed dynamics in the interaction region [**6**].

Where, E_o, and E_1: the intensity of the zero and first orders, respectively, b: is the Bragg line.

Fox in 1982 [7], showed that the equations describing the interaction between an optical beam and an acoustic wave are derived using plane waves derived from elementary scattering sources. The obtained results are in good agreement with other well known methods such as the differential difference equation approach.

The equations are applied to the acousto-optic interaction in the weak and strong approximations and also to the scattering of finite-width optical beams with rectangular and Gaussian profiles.

Berg in 1983[**5**], developed many acousto-optical devices for signal processing as light modulators, deflectors, filters and analyzers were applied in science and technology as well as in practical opto-electronics, photonics etc.

Zadorin and Sharangovich in 1987 [**8**], showed that the acousto-optic interaction of complex optical and acoustic radiation fields in a crystal is investigated. Differential equations are obtained for the diffracted light field in anisotropic medium. The problem of strong acousto-optic interaction in the field of a focused acoustic wave is solve. The solutions describe the diffracted field near the acoustic lens and also in the vicinity of its focus.

Brooks and Reeve in 1995 [**9**], showed the ability of an AO cell to deflect a light beam through an angle proportional to the frequency applied to its transducer has been exploited to construct a simple effective “FM” demodulator. Two different types of detector are considered: a single detector and a Bi-cell detector. The performance of the bi-cell system is found to be superior by virtue of its ability to reduce/cancel the effects of amplitude modulation on the signal and variations in laser intensity. It is shown that

systems can be designed to operate at center frequencies from tens of MHz to a few GHz, with maximum frequency deviations and modulation frequencies from a few KHz to tens of MHz. Experimental results are presented to demonstrate the validity of these expressions. It is concluded that an AO system may be use to measure the “FM” characteristics of a signal.

Sharangovich in 1995 [**10**], Showed a theoretical model is presented for the strong two-dimensional acousto-optic interaction “AOI” of finite size beams with arbitrary profiles in an acoustic field with a curved wave front. Transfer functions are derived in a universal normalized form for the AOI. The results of numerical simulation of the diffraction characteristics show that during AOI in an acoustic field with a curved wave front the product of the diffraction efficiency and band width increases at least 1.5 times for a weak interaction and more than five times for a strong interaction.

Thompson in 1996 [**11**], showed the interaction between SAWs and guided optical waves in Si Ge/Si structure by determining the electric field of the optical mode, the strain that induced by propagating SAW.

Dunn and Poon in 1997 [**12**], presented analytical solution to the strong acousto-optic interaction problem in three dimensions and compare the analytical results to two different split-step numerical algorithms. The first algorithm uses the concept of Fourier-optics, while the second relies on the more rigorous wave equation approach.

Derek in 1998 [**13**], explained the image processing by acousto-optic Bragg diffraction to perform image enhancement. Theoretical results consists two

diffracted order in three dimensions. The presented experimental data confirms the validity of the theoretical results.

Arshia and Poon in 2003[**14**], showed an AOM consists of a small piece of crystal or glass to which a piezo-electric transducer is bonded. When a voltage waveform is applied to the transducer, an AOM can be made to intensity modulate, frequency shift or deflect a laser beam through the AO effect.

A bi-stable device was a device with a capability to generate two different outputs for a given input. In this study used first-order diffracted light as feedback. The nonlinearity associated with the AOM and the feedback causes bi-stability in the overall system. For this goal mathematical and analytical models describing the AO interaction were numerically solved by using MATLAB.

Masalsky in 2003 [**15**], explained that the waveguide acousto-optic unit based on Bragg diffraction of the modulated light beam, so that this device is widely used in many field like computing, telecommunication.

The theoretical analysis showed that the waveguide exist for diffracted and un diffracted optical waves.

Hang in 2004 [**16**], studied optic-acoustic “OA” imaging as an emerging technology that combines the high contrast of tissue optical properties and the high spatial resolution of ultrasound. In this study we assumed a new numerical

Approach based on the Finite Difference Time-Domain “FDTD” method to solve the general OA equations.

Obaidy in 2005 [**17**], studied a computer simulation by using MATLAB software to deduce the value of design parameters such as Klein-Cook "Q" parameter and crystal efficiency at the acoustic frequencies. Experimental work involves two parts:

1. The optical part used Lithium Niobate "$LiNbO_3$" crystal as nonlinear crystal and He-Ne laser of 632.8 nm wavelength and 1 mw output power.
2. The electrical part which is constructs the trigger circuit and high voltage.

The result showed that the condition Q>1 means that the crystal operates in Bragg regime. Also, introducing the relation between peak phase delay "α" and laser intensity at different values of Q of the fourth diffraction orders to describe the light-sound interaction in the crystal.

Tsarev in 2007 [**18**], studied the numerical simulation of acoustics-optics tunable filters based on multi- reflection beam. Planer waveguide filters based on the thin film of $LiNbO_3$ by using FDTD method. The results showed that the AO filters have very good dispersion properties and extremely small size provide a narrow filtration line.

Molchanov and Makarov in 2007 [**19**], showed that the theoretical and experimental investigation of acousto-optical tunable filters, based on quasi-collinear geometry of light-sound interaction in tellurium dioxide single crystal. This configuration uses the effect of strong acoustic anisotropy in tellurium dioxide as well as peculiarities of acoustic wave reflections from the free boundary of the crystal.

Baryshev and Epikhin in 2010[**20**], showed that new acousto-optic modulator (AOM-RN) operating purely in the Raman-Nath diffraction regime.

This device can be used as an external phase modulator in frequency-modulation (FM) optical heterodyne spectroscopy for fast and broadband frequency control of diode lasers. The FM spectroscopy based on AOM-RN makes it possible to analyze both absorption and dispersion properties of optical resonances under study; this possibility is shown by the example of saturated-absorption resonances in cesium vapor. The possibility of detecting coherent population trapping resonances using FM spectroscopy with AOM-RN as an external phase modulator is experimentally demonstrated.

1.7 The aim of thesis

The aim of this work is to simulate the properties of an Acousto-Optic Modulator “AOM”. The simulation procedure is based on theoretical and computational relationships describing acousto-optic properties of the AO cell parameters. Three different materials have been used, which are “Glass, Germanium, and Tellurium-Oxide”. The AOM are calculated using two different techniques these are: Partial differential and Finite Difference Time Domain, algorithms.

1.8 Thesis layout

The thesis layout is as follows:

Chapter One

Involves general introduction and historical review of the previous published researches.

Chapter Two

Consist of a theoretical background for the thesis subject. Shows the two types of diffraction and characteristics of the diffracted light, also consist the brief description of the acousto-optic modulation and the modern application of acousto-optic effect.

Chapter Three

Involves the results drawn on graphs in 2-D coordinate for the intensity of the diffracted orders versus peak phase delay for Glass, Germanium, and Tellurium-Oxide crystals using partial differential equation.

Chapter Four

Involve the results drawn on graphs in 2-D and 3-D coordinates for the intensity of the electric field versus the time propagation and electro magnetic wave propagation for Glass, Germanium, and Tellurium-Oxide crystals using Finite Difference Time Domain.

Chapter Five

Involves conclusions of this work and the suggestions for the future works.

CHAPTER THREE

Theoretical Computation

3.1 Introduction

A partial differential equations "PDE" is an equation that contains partial derivatives. In contrast to ordinary differential equations "ODE", where the unknown function depends only on one variable, while in PDE the unknown depends on several variables. A PDE are useful method because all nature laws of physics like the Maxwell's equation, Newton's law of cooling, Newton's law of motion, and Schrodinger's equation of quantum mechanics are stated in terms of PDE. These laws describe physical phenomena by relating space and time derivatives [**29**]. In this chapter, we propose a numerical approach based on the partial differential equations to calculate the intensity of the diffracted orders "ψ" versus peak phase delay "α".

3.2 Theoretical part

In this section solve a partial differential equation which describes the intensity for the different diffracted orders. This is known as Korpel-Poon equation which is given by [**1**]:

$$\frac{d\psi_m}{d\xi} = -j\frac{\alpha}{2}e^{-j\frac{1}{2}Q\xi\left[\frac{\emptyset_{inc}}{\emptyset_B}+(2m-1)\right]}\psi_{m-1} - j\frac{\alpha}{2}e^{j\frac{1}{2}Q\xi\left[\frac{\emptyset_{inc}}{\emptyset_B}+(2m+1)\right]}\psi_{m+1} \qquad 3.1$$

Equation (3.1) could be used to demonstrate some numerical results obtained by MATLAB. The set of the ten coupled differential equations stated below satisfy Eq. (3.1). These differential equations are given as follows [**1**]:

From Eq. (3.1), the 5th, 4th, 3rd, 2nd, and 1st diffracted orders are given by [**1**]:

$$\frac{d\psi_5}{d\xi} = -j\frac{\alpha}{2}e^{-j\frac{1}{2}Q\xi\left[\frac{\emptyset_{inc}}{\emptyset_B}+9\right]}\psi_4 - 0$$

$$\frac{d\psi_4}{d\xi} = -j\frac{\alpha}{2}e^{-j\frac{1}{2}Q\xi\left[\frac{\emptyset_{inc}}{\emptyset_B}+7\right]}\psi_3 - j\frac{\alpha}{2}e^{j\frac{1}{2}Q\xi\left[\frac{\emptyset_{inc}}{\emptyset_B}+9\right]}\psi_5$$

$$\frac{d\psi_3}{d\xi} = -j\frac{\alpha}{2}e^{-j\frac{1}{2}Q\xi\left[\frac{\emptyset_{inc}}{\emptyset_B}+5\right]}\psi_2 - j\frac{\alpha}{2}e^{j\frac{1}{2}Q\xi\left[\frac{\emptyset_{inc}}{\emptyset_B}+7\right]}\psi_4 \qquad 3.2$$

$$\frac{d\psi_2}{d\xi} = -j\frac{\alpha}{2}e^{-j\frac{1}{2}Q\xi\left[\frac{\emptyset_{inc}}{\emptyset_B}+3\right]}\psi_1 - j\frac{\alpha}{2}e^{j\frac{1}{2}Q\xi\left[\frac{\emptyset_{inc}}{\emptyset_B}+5\right]}\psi_3$$

$$\frac{d\psi_1}{d\xi} = -j\frac{\alpha}{2}e^{-j\frac{1}{2}Q\xi\left[\frac{\emptyset_{inc}}{\emptyset_B}+1\right]}\psi_0 - j\frac{\alpha}{2}e^{j\frac{1}{2}Q\xi\left[\frac{\emptyset_{inc}}{\emptyset_B}+3\right]}\psi_2$$

While, the zeroth diffracted order is given by [**1**]:

$$\frac{d\psi_0}{d\xi} = -j\frac{\alpha}{2}e^{-j\frac{1}{2}Q\xi\left[\frac{\emptyset_{inc}}{\emptyset_B}-1\right]}\psi_{-1} - j\frac{\alpha}{2}e^{j\frac{1}{2}Q\xi\left[\frac{\emptyset_{inc}}{\emptyset_B}+1\right]}\psi_1 \qquad 3.3$$

While, the -1, -2, -3, -4 diffracted orders are given by [**1**]:

$$\frac{d\psi_{-1}}{d\xi} = -j\frac{\alpha}{2}e^{-j\frac{1}{2}Q\xi\left[\frac{\emptyset_{inc}}{\emptyset_B}-3\right]}\psi_{-2} - j\frac{\alpha}{2}e^{j\frac{1}{2}Q\xi\left[\frac{\emptyset_{inc}}{\emptyset_B}-1\right]}\psi_0$$

$$\frac{d\psi_{-2}}{d\xi} = -j\frac{\alpha}{2}e^{-j\frac{1}{2}Q\xi\left[\frac{\emptyset_{inc}}{\emptyset_B}-5\right]}\psi_{-3} - j\frac{\alpha}{2}e^{j\frac{1}{2}Q\xi\left[\frac{\emptyset_{inc}}{\emptyset_B}-3\right]}\psi_{-1} \qquad 3.4$$

$$\frac{d\psi_{-3}}{d\xi} = -j\frac{\alpha}{2}e^{-j\frac{1}{2}Q\xi\left[\frac{\emptyset_{inc}}{\emptyset_B}-7\right]}\psi_{-4} - j\frac{\alpha}{2}e^{j\frac{1}{2}Q\xi\left[\frac{\emptyset_{inc}}{\emptyset_B}-5\right]}\psi_{-2}$$

$$\frac{d\psi_{-4}}{d\xi} = 0 - j\frac{\alpha}{2}e^{j\frac{1}{2}Q\xi\left[\frac{\emptyset_{inc}}{\emptyset_B}-7\right]}\psi_{-3}$$

3.3 Numerical Results

In this section, the numerical results for the intensity of the diffracted orders (ten orders) where -4<m<5 versus peak phase delay have been calculated using computer program written with MATLAB simulation using partial differential equation to solve Eq. (3.1). In this research have been used three different materials, which are Glass, Germanium, and Tellurium-Oxide.

Tables (3.1), (3.2) and (3.3) demonstrating the properties of the above these materials.

Table (3.1) represents the properties of the Glass material [**30**]

Table (3.1): properties of the Glass material [30]	
1- Operating wavelength	440-633 nm
2- Acoustic velocity	3509 m/s
3- Active aperture	1.7 mm
4- Center frequency	40 MHz
5- Input impedance	50 Ω
6- Radio frequency band width (RF)	20 MHz
7- Bragg angle	2.5 mrad at 442 nm 3 mrad at 515 nm 3.6 mrad at 633 nm
8- Diffraction efficiency	90 %

while, table (3.2) represents the properties of Germanium material [**30**]

Table (3.2): Properties of the Germanium material [30]	
1- Operating wavelength	10.6 μm
2- Acoustic velocity	5500 m/s
3- Active aperture	3 mm
4- Center frequency	40MHz
5- Input impedance	50 Ω
6- RF band width	16 MHz
7- Bragg angle	38.5 mrad
8- Diffraction efficiency	>80 %

while, table (3.3) represents the properties of Tellurium-Oxide material [**30**]

Table (3.3): Properties of the Tellurium-Oxide material [30]	
1- Operating wavelength	532 nm
2- Acoustic velocity	650 m/s
3- Active aperture	2 mm
4- Center frequency	80 MHz
5- Input impedance	50 Ω
6- RF band width	40 MHz
7- Bragg angle	0.023π mrad
8- Diffraction efficiency	85 %

The interaction lengths “D” for each material and Klein-Cook parameter “Q” are calculated using Eq. (1.6) are shown in table (3.4).

Table (3.4): The values of interaction length “D” and Klein-Cook parameter “Q” for the Glass, Germanium, and Tellurium-Oxide crystals

Glass Crystal		Germanium Crystal		Tellurium-Oxide Crystal	
D - meter	Q	D - meter	Q	D - meter	Q
0.04	9.62	0.04	0.89	0.04	22.7
0.05	12.0	0.05	1.11	0.05	28.3
0.06	14.4	0.06	1.34	0.06	34.0
0.07	16.8	0.07	1.56	0.07	39.7
0.08	19.2	0.08	1.78	0.08	45.4
0.09	21.6	0.09	2.0	0.09	51.0
0.1	24.0	0.1	2.23	0.1	56.7

Figure (3.1) shows the relation between klein-cook parameter with interaction lengths for the Glass, Germanium and Tellurium-Oxide crystals.

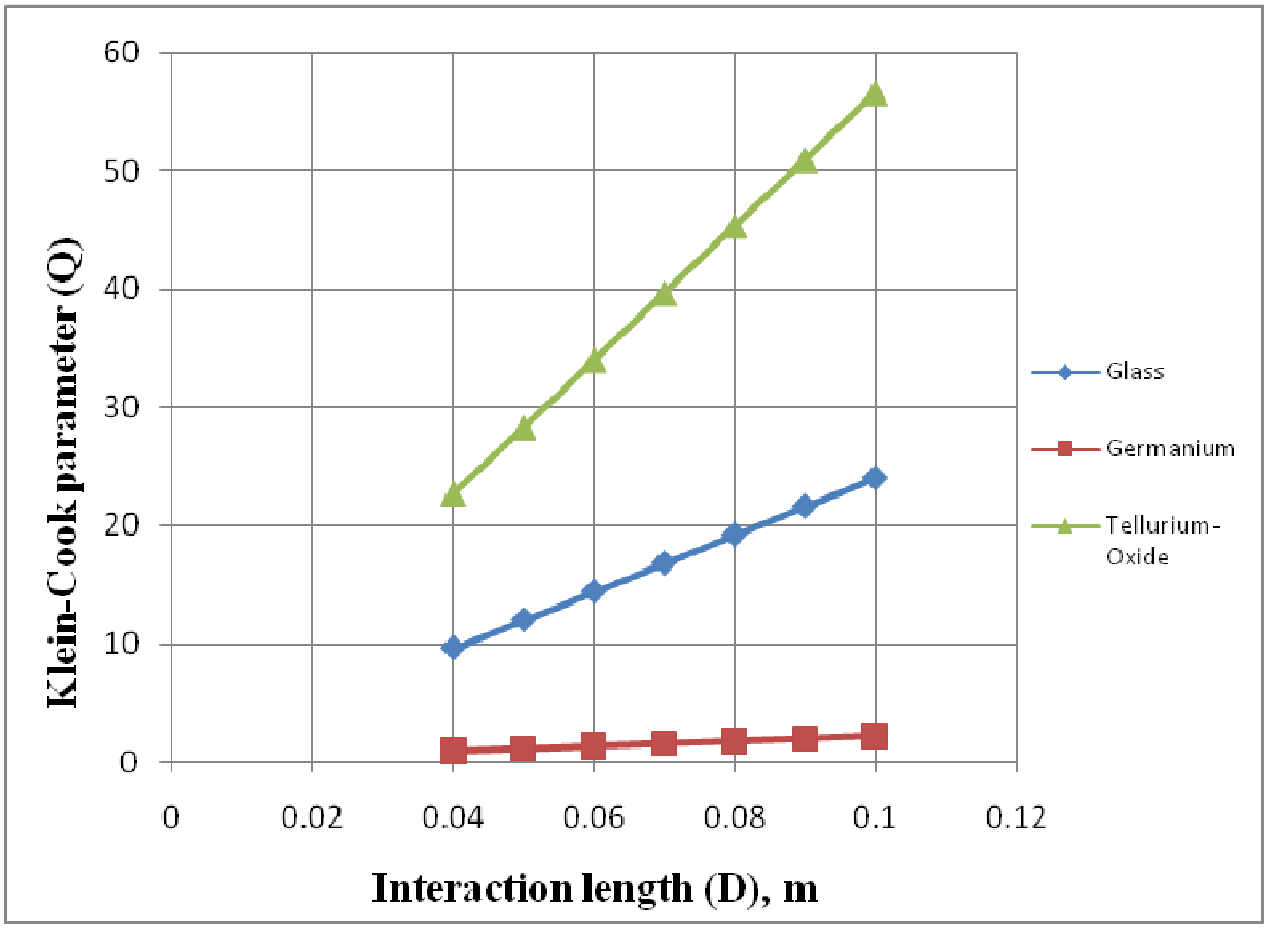

Figure (3.1): Klein-Cook parameter versus interaction length for Glass, Germanium and Tellurium-Oxide crystals.

Figures (3.2), (3.3), and (3.4) shows the numerical results for the normalized intensity "ψ", for the diffracted orders "m"; m = -1, 0, 1 versus peak phase delay "α", for Glass material, in case of D=0.05: Q=12, D=0.07 m: Q=16.8, and D=0.1 m: Q=24, respectively.

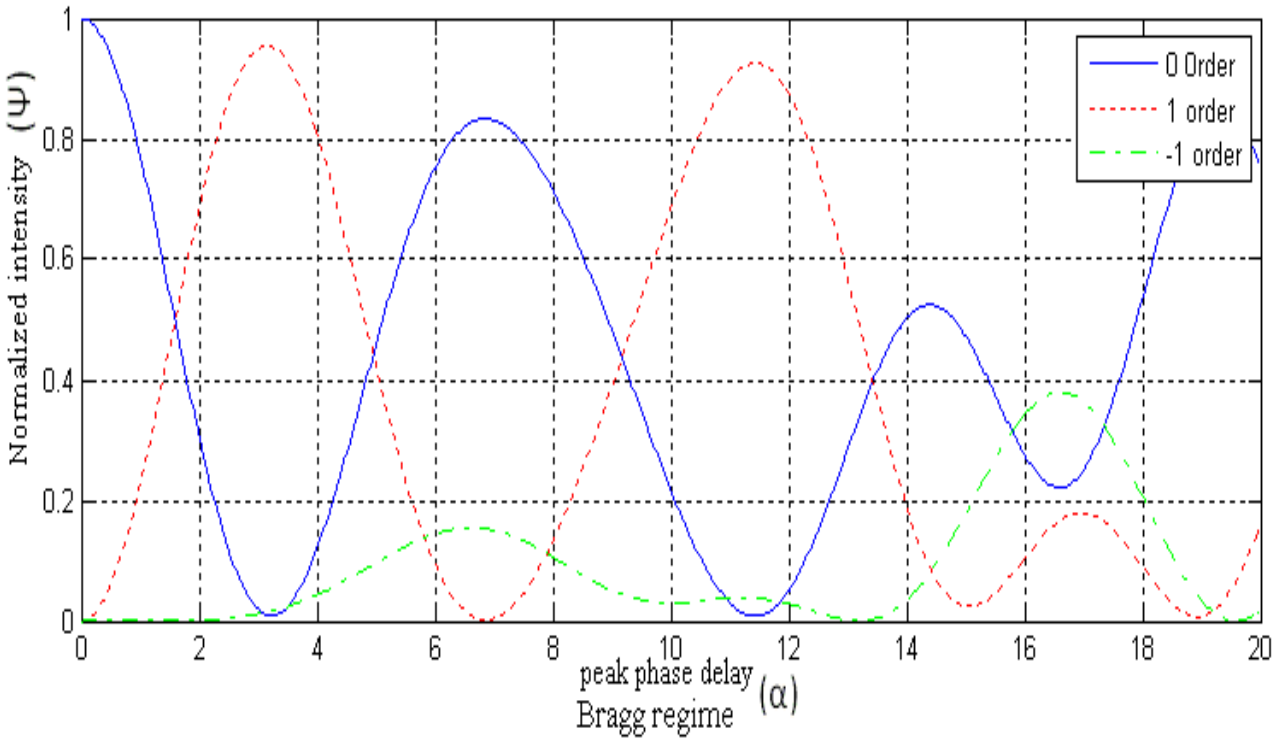

Figure (3.2): Normalized intensity of the diffracted orders versus peak phase delay for D=0.05m, Q=12 of Glass crystal

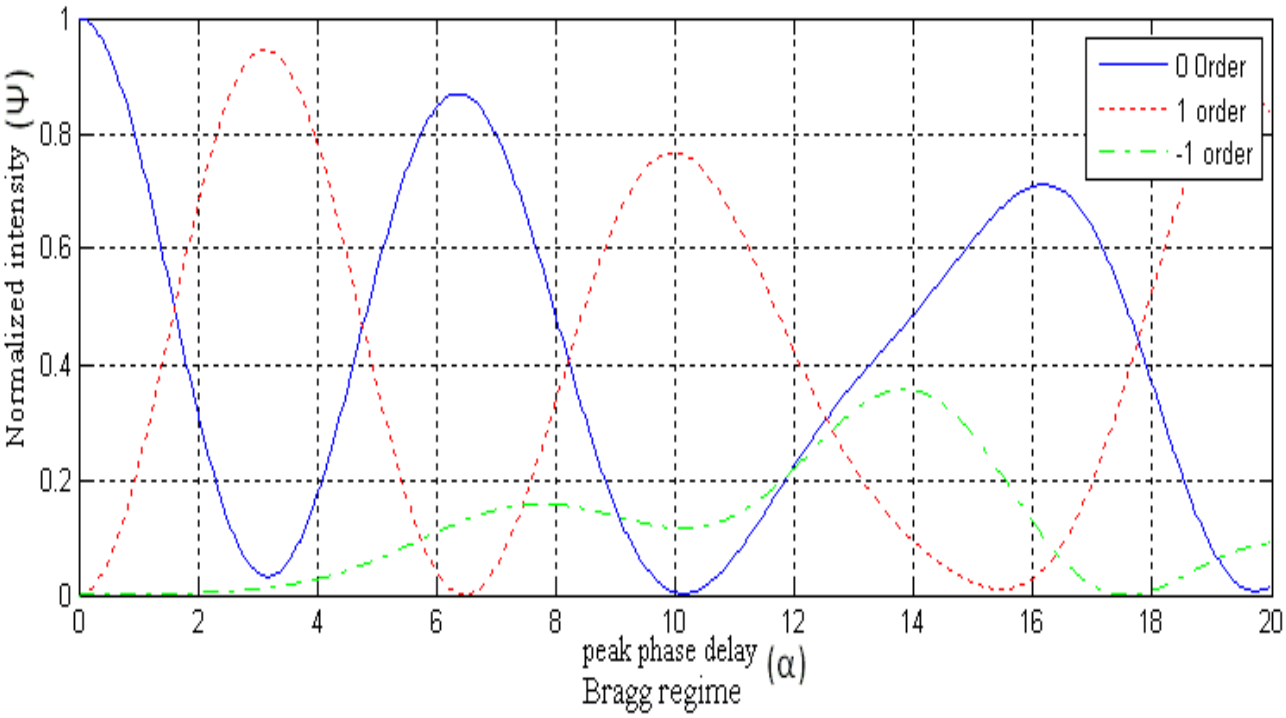

Figure (3.3): Normalized intensity of the diffracted orders versus peak phase delayfor D=0.07m, Q=16.8 of the Glass crystal

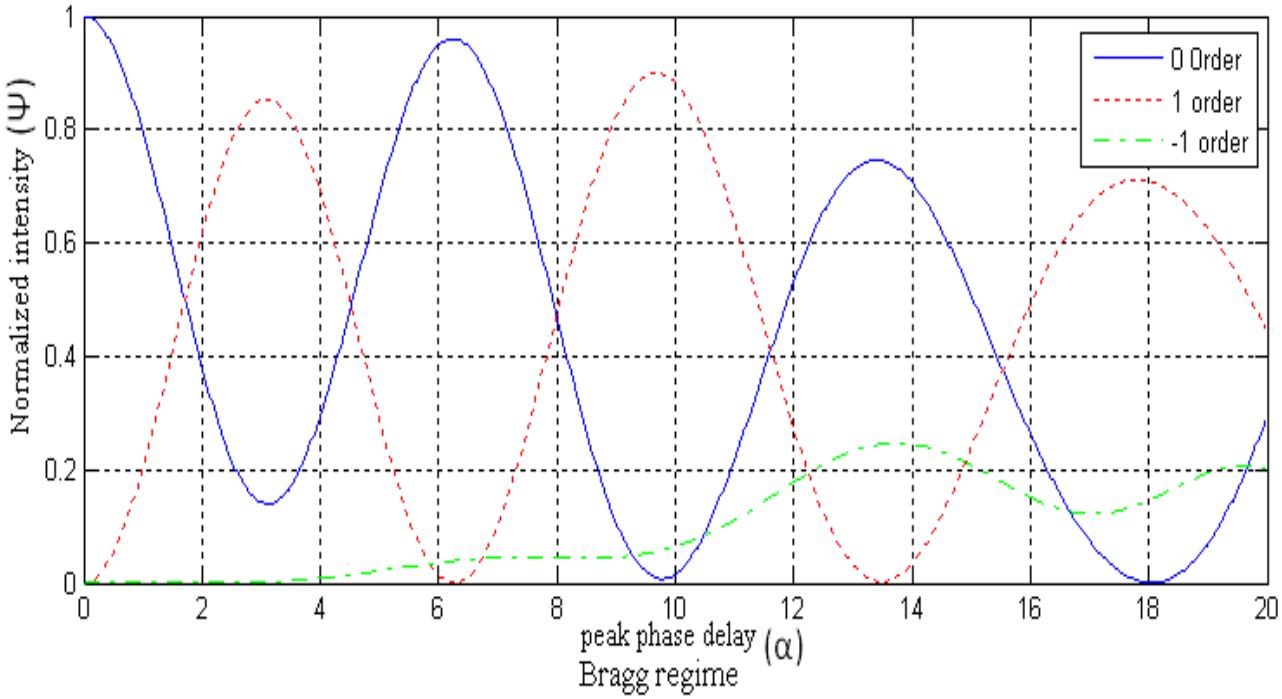

Figure (3.4): Normalized intensity of the diffracted orders versus peak phase delay for D=0.1m, Q=24 of Glass crystal

From the above figures one can see that the values of Q are greater than 1, and for this situation the state is called **Bragg** regime. From the above results, we can see that the intensity exchanges are higher for zero and first orders than for (-1) order. Also, the intensity decreases with the increasing the interaction length.

Figures (3.5), (3.6), (3.7), and (3.8) shows the numerical results for the normalized intensity "ψ", for the diffracted orders "m"; m=-5, -2, -1, 0, 1, 2, 5 versus peak phase delay "α", for Germanium material, in case of D=0.04 m: Q=0.89, D=0.05 m: Q=1.11, D=0.07 m: Q=1.56, and D=0.1 m: Q=2.23, respectively.

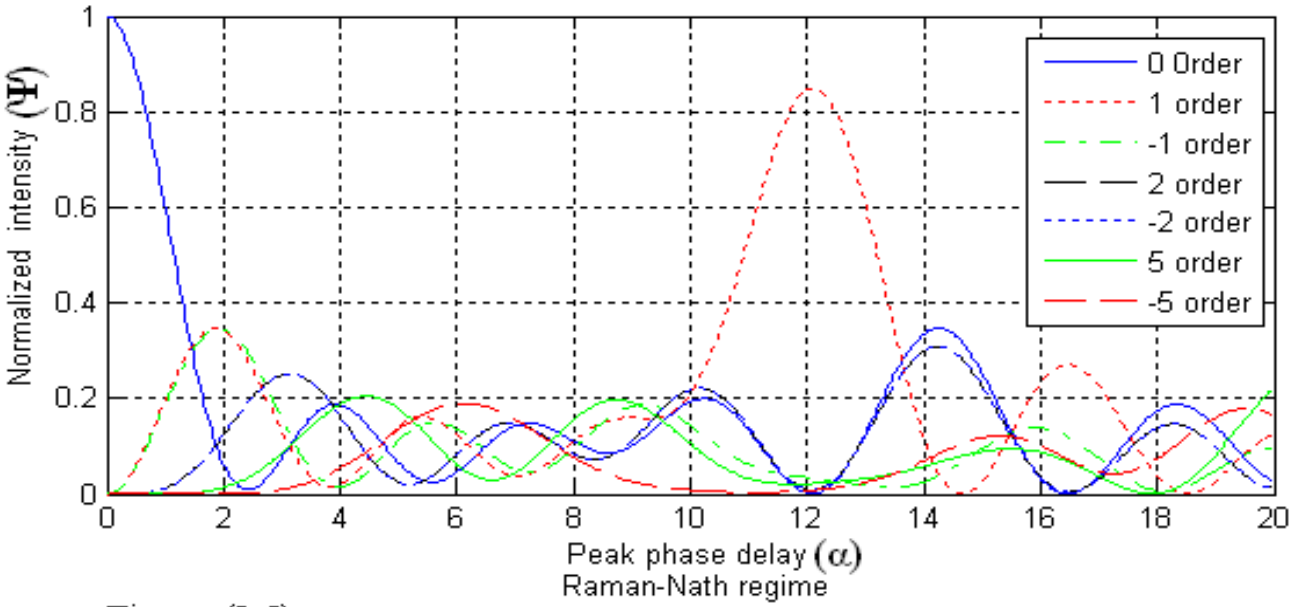

Raman-Nath regime

Figure (3.5): Normalized intensity of the diffracted orders versus peak phase delay D=0.04 m,Q=0.89 for Germanium crystal

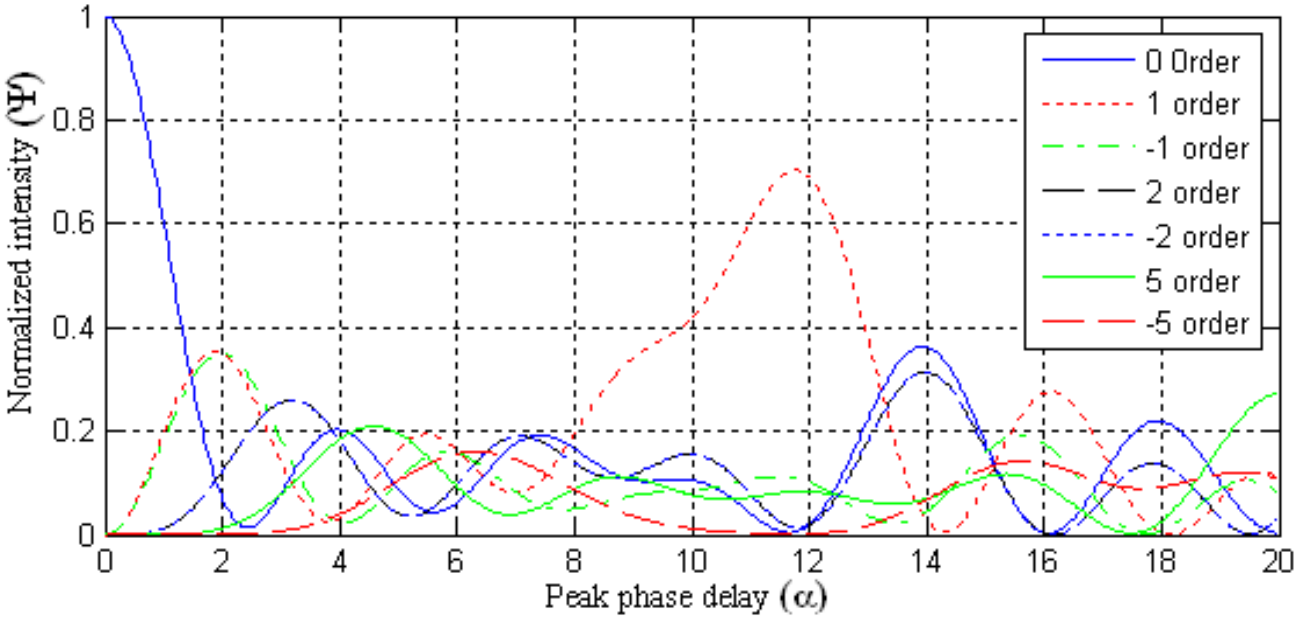

Non ideal Raman-Nath regime

Figure (3.6): Normalized intensity of the diffracted orders versus peak phase delay D=0.05 m,Q=1.11 for Germanium crystal

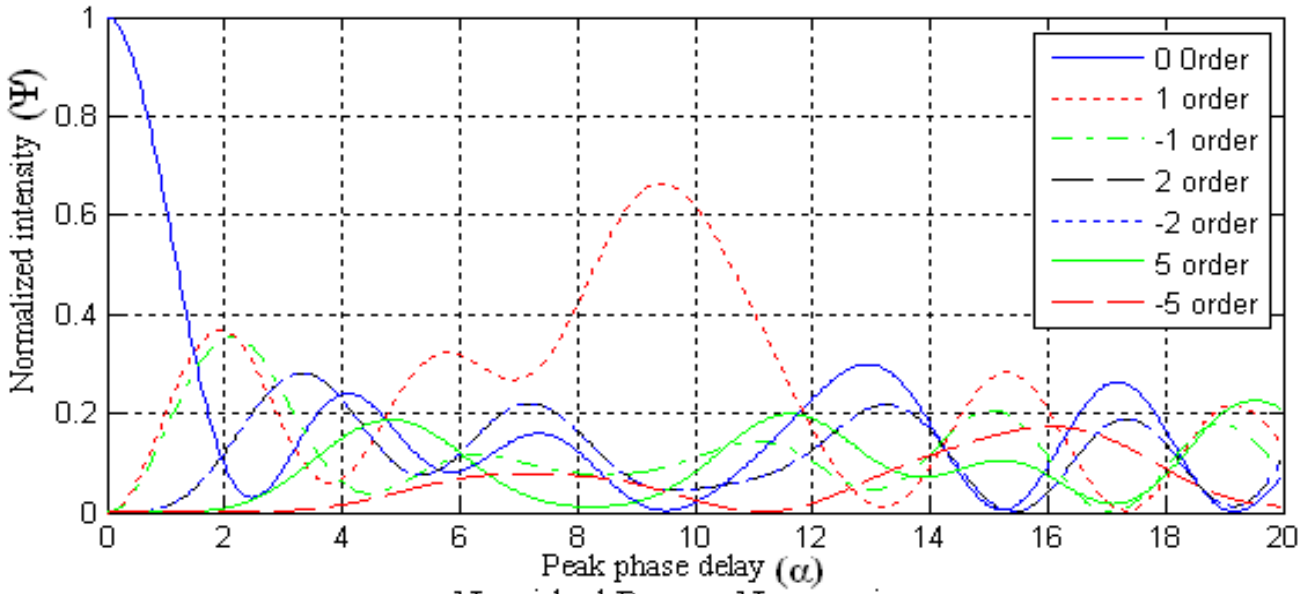

Non ideal Raman-Nath regime

Figure (3.7): Normalized intensity of the diffracted orders versus peak phase delay D=0.07 m,Q=1.56 for Germanium crystal

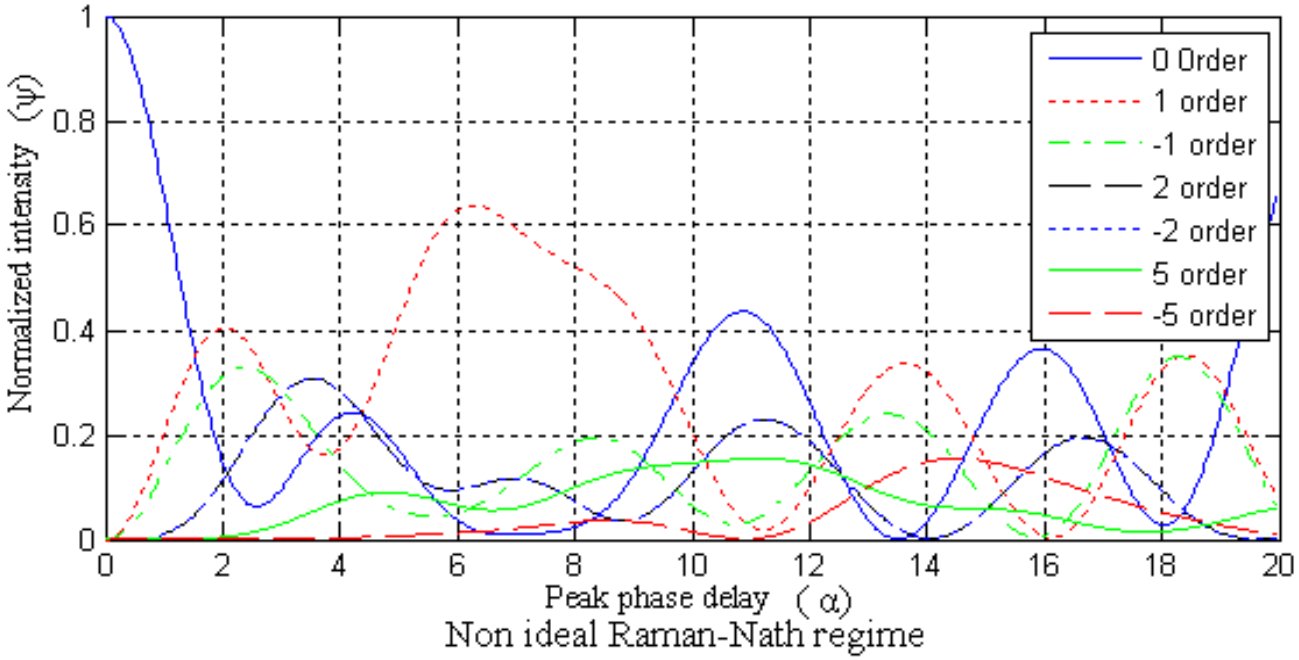

Non ideal Raman-Nath regime

Figure (3.8): Normalized intensity of the diffracted orders versus peak phase delay D=0.1 m,Q=2.23 for Germanium crystal.

From the figure (3.5) one can see that the value of Q is less than 1, which is called ideal **Raman-Nath** regime. While figures (3.6), (3.7) and (3.8) shows that the values of Q are little greater than 1, this situation is called non-ideal **Raman-Nath** regime. Moreover, we see that the exchanges of intensity are higher for zero and first orders. Furthermore, the first order decreases with increasing the Q parameter.

Figures (3.9), (3.10) and (3.11) shows the numerical results for the normalized intensity "ψ" for the diffracted orders "m"; m= -1, 0 1 versus peak phase delay "α", for Tellurium-Oxide material in case of D=0.05 m:Q=28.3, D=0.07 m: Q=39.7, and D=0.1 m: Q=56.7, respectively.

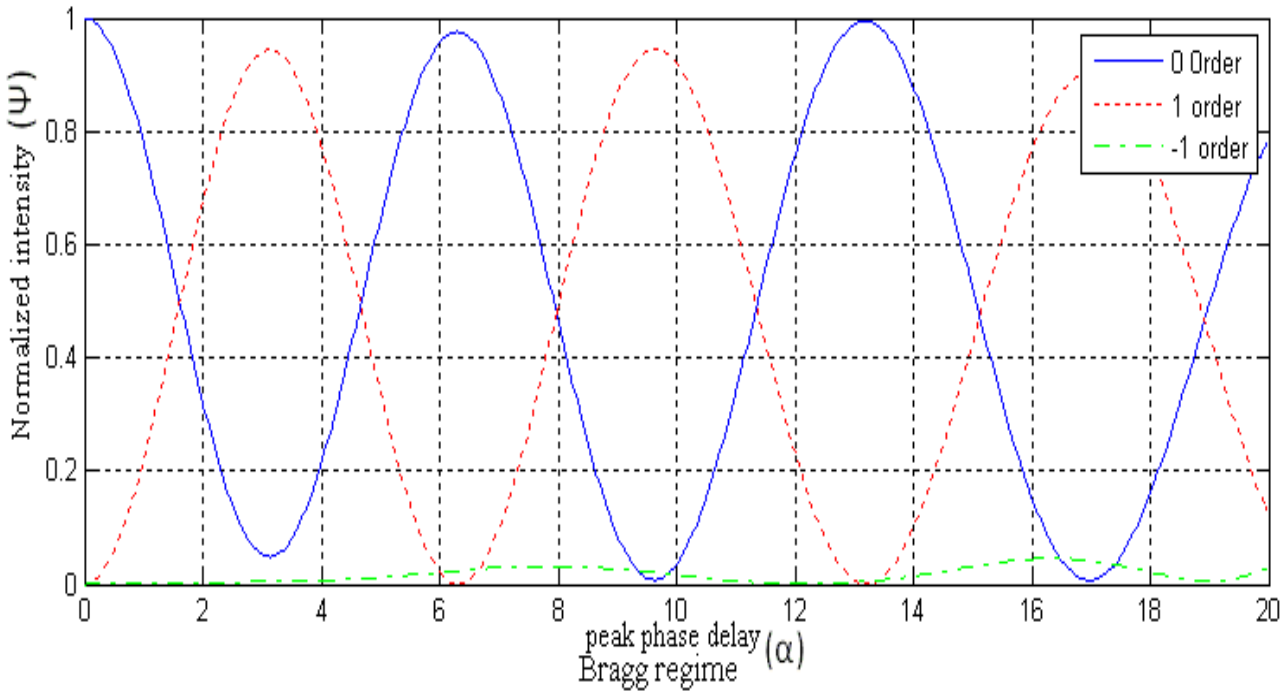

Figure (3.9): Normalized intensity of the diffracted orders versus peak phase delay for D=0.05m,Q=28.3 of Tellrium-Oxide crystal

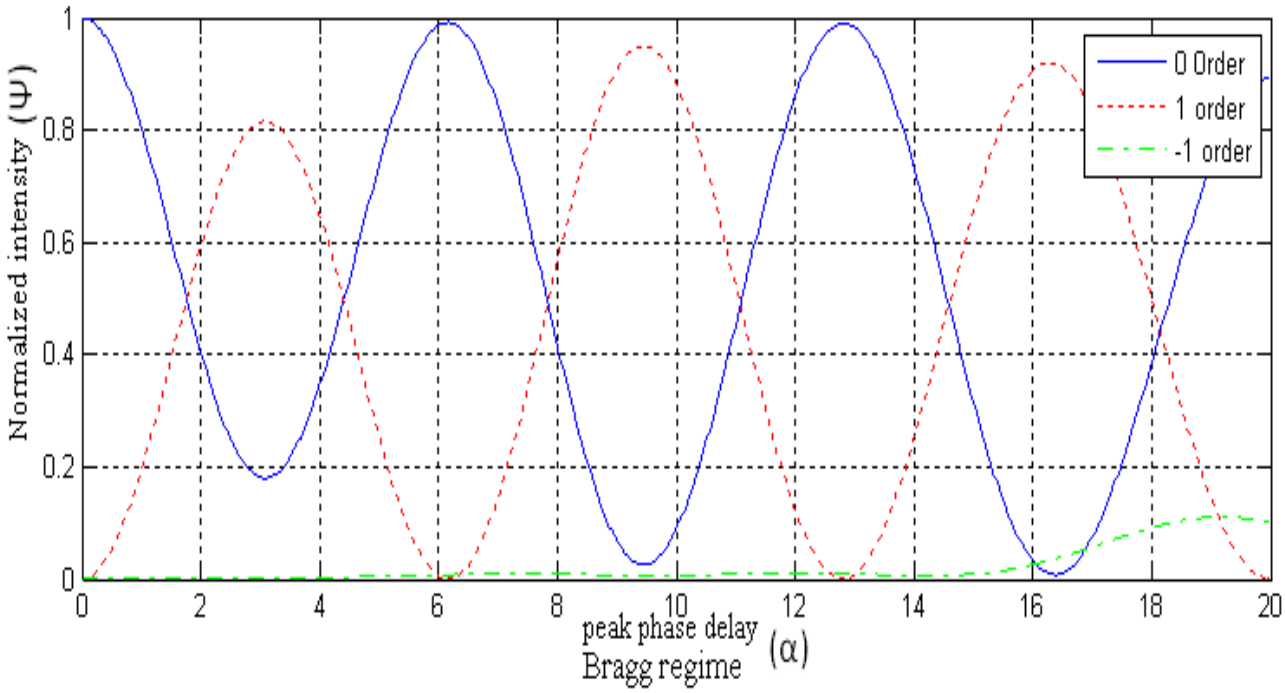

Figure (3.10): Normalized intensity of the diffracted orders versus peak phase delay for D=0.07 m,Q=39.7 of Tellrium-Oxide crystal

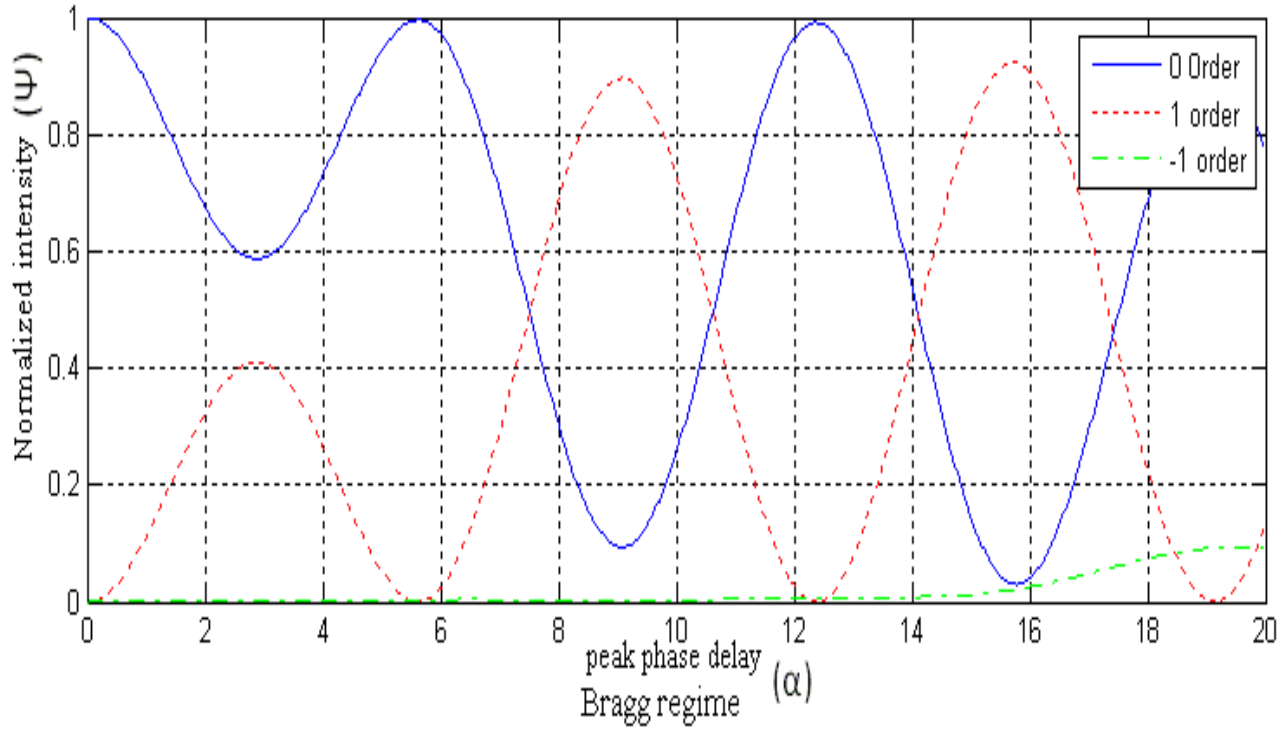

Figure (3.11): Normalized intensity of the diffracted orders versus peak phase delay for D=0.1 m,Q=56.7 of Tellrium-Oxide crystal

From the above figures show that the values of Q are greater than 1, that is called **Bragg** regime. The comparison between these materials shows that the values of Q for Tellurium-Oxide are greater than the Glass and Germanium materials. Therefore, the (-1) orders disappear in the Tellurium-Oxide material. While for Glass material the (-1) orders show little appearance. The phase difference between first and zero orders was 180^{o} in Tellurium-Oxide material and Glass materials. Moreover, the intensity of diffracted orders decreases with the increasing of Q .

3.4 Conclusions:

The results for the Glass material and Tellurium-Oxide material shows that the periodic exchange of intensity between the two main diffracted orders, which are zero and first, becomes smaller with the increasing the Q parameter. This indicates that the higher orders disappear in these materials because these above materials operates in **Bragg** regime and must be have values of Q are greater than 1 While, the results for Germanium material shows that the peak intensity exchange for the zero diffracted order vanish quickly and coincidence with the higher diffracted orders. From the above results we notice that the Tellurium-Oxide material was the best material more than Glass and Germanium materials because it has large values of Q. Moreover, -1 diffracted order may disappear, so that it satisfies the condition of Bragg regime more than other materials.

CHAPTER TWO

Theory of Acousto-Optics

2.1 Theoretical Approach

Brillouin in 1922 predicted the diffraction of the light beam by ultrasonic waves which is called ***Acousto optic*** "AO". The effect of acousto-optic can be described as follows: An ultrasonic wave propagating through a solid or liquid locally causes compression and rarefaction of the medium. This compression and rarefaction of the medium is known as a ***photo elastic effect*** and this effect changes the refractive index of the medium [**13**].

2.2 General Formalism of Acousto-Optic Effect

The interaction between the electric fields $\mathbf{E}_o(\mathbf{R},t)$ and sound field $\mathbf{S}(\mathbf{R},t)$ can be described by Maxwell equations. It is typically assumed that the interaction takes place in an optically inhomogeneous, nonmagnetic isotropic medium characterized by permeability "μ_o" and a permittivity $\epsilon(\mathbf{R},t)$. The time-varying permittivity is given by [**1**]:

$$\epsilon_{(R,t)} = \epsilon + \epsilon'(R,t) \qquad 2.1$$

where $\epsilon'(R,t) = \epsilon\, b\, S(\mathbf{R},t)$, i.e. it is proportional to the sound field amplitude $S(\mathbf{R},t)$, with "b" the proportionality constant of the medium, ϵ is the permittivity of crystals. Hence; notice that $\epsilon'(R,t)$ represents the action in permittivity of the sound field. We will assume the incident light field $\mathbf{E}_{inc}(\mathbf{R},t)$ satisfies Maxwell equations, with charge density "ρ" and current density "**J**"

equal zero. When the sound field interacts with $\mathbf{E}_{inc}(R,t)$ the total light fields $\mathbf{E}(\mathbf{R},t)$ and $\mathbf{H}(\mathbf{R},t)$ in the acoustic medium should also satisfy Maxwell equations is given by [**1**]:

$$\nabla x\mathbf{E}(\mathbf{R},t) = -\mu_o \frac{\partial \mathbf{H}(\mathbf{R},t)}{\partial t} \quad 2.2$$

$$\nabla x\mathbf{H}(\mathbf{R},t) = \frac{\partial}{\partial t}[\epsilon(\boldsymbol{R},t)\boldsymbol{E}(\boldsymbol{R},t)] \quad 2.3$$

$$\nabla.[\epsilon(\boldsymbol{R},t)\boldsymbol{E}(\boldsymbol{R},t)] = 0 \quad 2.4$$

$$\nabla.\boldsymbol{H}(\boldsymbol{R},t) = 0 \quad 2.5$$

Where $\mathbf{E}(\mathbf{R},t)$ is the electric field and $\mathbf{H}(\mathbf{R},t)$ is the magnetic field.

Taking the curl of Eq. (2.2) and introducing it into Eq. (2.3), the equation for $\mathbf{E}(\mathbf{R},t)$ becomes :

$$\nabla x\nabla x\mathbf{E}(\mathbf{R},t) = \nabla x - \mu_o \frac{\partial \boldsymbol{H}(\boldsymbol{R},t)}{\partial t} = -\mu_o \frac{\partial}{\partial t}\nabla x\mathbf{H}(\mathbf{R},t) \quad 2.6$$

$$= -\mu_o \frac{\partial}{\partial t}\left(\frac{\partial}{\partial t}\epsilon(\boldsymbol{R},t)\boldsymbol{E}(\boldsymbol{R},t)\right) \quad 2.7$$

$$\nabla x\nabla x\mathbf{E}(\mathbf{R},t) = \nabla(\nabla.\mathbf{E}) - \nabla^2\mathbf{E} = -\mu_o \frac{\partial^2}{\partial t^2}[\epsilon(\mathbf{R},t)\mathbf{E}(\mathbf{R},t)] \quad 2.8$$

Now, from Eq.(2.4), we have:

$$\nabla.\epsilon\boldsymbol{E} = \epsilon\nabla.\boldsymbol{E} + \boldsymbol{E}.\nabla\epsilon = 0 \quad 2.9$$

Assuming a two-dimensional (x-z) sound field with **E** polarized along the y-direction, i.e.**, E(r,t) = E**(**r**,t)y we can readily show that **E**.$\nabla\epsilon(R,t)$ =0. Hence equation (2.9) reduces to:

$$\nabla^2\boldsymbol{E}(\boldsymbol{R},t) = \mu_o \frac{\partial^2}{\partial t^2}[\epsilon(\boldsymbol{R},t)\boldsymbol{E}(\boldsymbol{R},t)] \qquad 2.10$$

where **R** is the position vector at x-z plane. in re-writing the term on the right hand side of Eq.(2.10) we get [**1**]:

$$\mu_o\left[\boldsymbol{E}\frac{\partial^2\epsilon}{\partial t^2} + 2\frac{\partial \boldsymbol{E}}{\partial t}\frac{\partial\epsilon}{\partial t} + \epsilon\frac{\partial^2\boldsymbol{E}}{\partial t^2}\right] \qquad 2.11$$

Neglecting the first and second terms from Eq.(2.11), because, the sound frequency is much lower than the light frequency. i.e. the time variation of the Є**(R,** t) is much slower than that of ***E*(R,** t) using Eq.(2.1) and Eq.(2.10) to get

$$\nabla^2\boldsymbol{E}(\boldsymbol{R},t) - \mu_o\epsilon\frac{\partial^2\boldsymbol{E}(\boldsymbol{R},t)}{\partial t^2} = \mu_o\epsilon'(\boldsymbol{R},t)\frac{\partial^2\boldsymbol{E}(\boldsymbol{R},t)}{\partial t^2} \qquad 2.12$$

Equation (2.12) is the wave equation that is often used to investigate strong interaction in AO. We can re-write Eq. (2.12) using Finite Difference Time-Domain FDTD by the form [**21**]:

$$\frac{\partial^2\boldsymbol{E}(\boldsymbol{x},t)}{\partial t^2} + \frac{\partial^2\boldsymbol{E}(\boldsymbol{z},t)}{\partial t^2} - \mu_o\epsilon\frac{\Delta^2\boldsymbol{E}(\boldsymbol{R},t)}{\Delta t^2} = \mu_o\epsilon'(\boldsymbol{R},t)\frac{\Delta^2\boldsymbol{E}(\boldsymbol{R},t)}{\Delta t^2} \qquad 2.13$$

Equation (2.13) can be written in other form as [21]:

$$\frac{\boldsymbol{E_{(x,t)\,i+1,j}-2E_{(x,t)\,i,j}+E_{(x,t)\,i-1,j}}}{h^2}+\frac{\boldsymbol{E_{(z,t)i+1,j}-2E_{(z,t)i,j}+E_{(z,t)i-1,j}}}{h^2}-$$

$$\mu_o\epsilon\left[\frac{\boldsymbol{E_{(x,t)i+1,j}-2E_{(x,t)\,i,j}+E_{(x,t)\,i-1,j}}}{\Delta t^2}+\frac{\boldsymbol{E_{(z,t)i+1,j}-2E_{(z,t)\,i,j}+E_{(z,t)i-1,j}}}{\Delta t^2}\right]-$$

$$\mu_o\epsilon'_{(\boldsymbol{r},\boldsymbol{t})}\left[\frac{\boldsymbol{E_{(x,t)\,i+1,j}-2E_{(x,t)i,j}+E_{(x,t)\,i-1,j}}}{\Delta t^2}+\frac{\boldsymbol{E_{(z,t)\,i+1,j}-2E_{(z,t)\,i,j}+E_{(z,t)\,i-1,j}}}{\Delta t^2}\right]=0 \qquad 2.14$$

2.3 Bragg Diffraction

Bragg diffraction is characterized by the generation of two scattered orders. In terms of Klien-Cook parameter Q should be far greater than one for operation in the Bragg regime. The zeroth order can only couple optical power into the plus or minus first order, i.e., there is phase matching between the zeroth and plus or minus first order. Laser beam light can't be transferred into the second or higher orders because there is no phase matching between these orders [**13**]. Another point that should be said about Bragg diffraction is that the interaction length, D, should be made large. All of the incident laser beam light is diffracted into a single order and satisfies this condition [**17**]:

$$\frac{\lambda}{\Lambda}\gg\frac{\Lambda}{D}\rightarrow D\gg\frac{\Lambda^2}{\lambda} \qquad 2.15$$

We have the following coupled equations describing the down-shifted interaction [**1**]:

$$\frac{d\psi_0}{dz}=-j\frac{\alpha}{2}\psi_{-1} \qquad 2.16$$

And

$$\frac{d\psi_{-1}}{dz} = -j\frac{\alpha}{2}\psi_0 \qquad 2.17$$

Similarly, the below two coupled equations described the up-shifted interaction.

$$\frac{d\psi_0}{dz} = -j\frac{\alpha}{2}\psi_1 \qquad 2.18$$

$$\frac{d\psi_1}{dz} = -j\frac{\alpha}{2}\psi_0 \qquad 2.19$$

where ψ is the intensity of the diffracted orders, j is the complex number, and α is the peak phase delay.

The diagram of Bragg diffraction can be represented as in Fig. (2.1) [**17**].

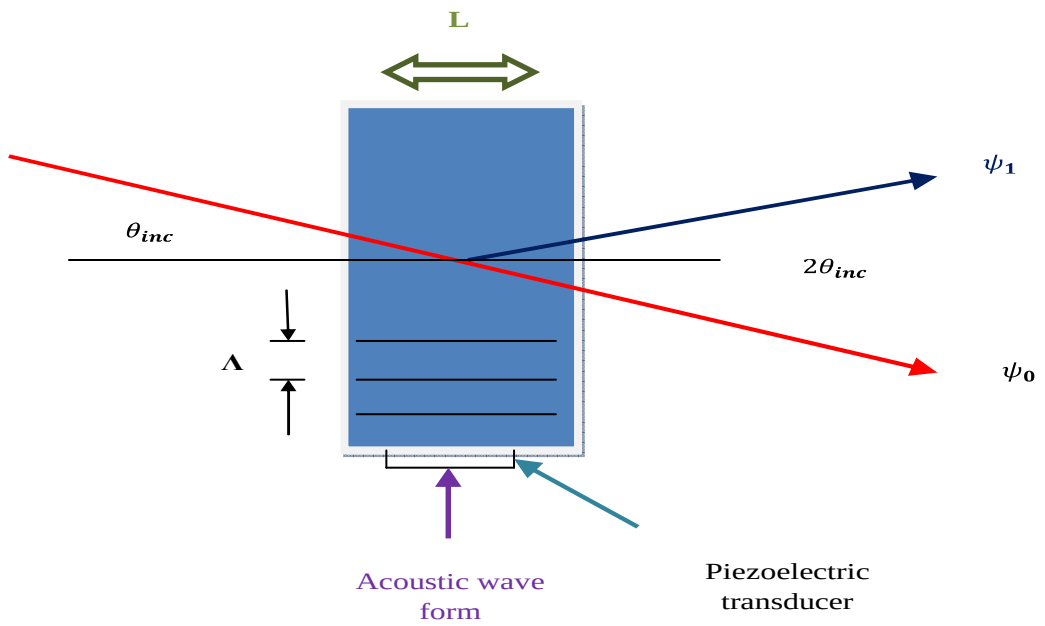

Figure (2.1): Bragg diffraction [**17**].

2.4 Raman-Nath Diffraction

Raman-Nath diffraction is characterized by the simultaneous generation of many scattered orders. Raman-Nath diffraction is also characterized by the operation of the AO cell with the angle of the incident laser light beam nearly equal to zero and choosing the Klein-Cook parameter Q to be much less than one [**13**]. This condition ensures that the interaction length "L" must be short enough and satisfies this condition [**17**]:

$$\frac{\lambda}{\Lambda} \ll \frac{\Lambda}{\lambda} \rightarrow L \ll \frac{\Lambda^2}{\lambda} \qquad 2.20$$

$$\frac{d\psi_m}{d\zeta} = -j\frac{\alpha}{2} e^{-j\frac{1}{2}Q\zeta\frac{\emptyset_{inc}}{\emptyset_B}} \psi_{m-1} - j\frac{\alpha}{2} e^{j\frac{1}{2}Q\zeta\frac{\emptyset_{inc}}{\emptyset_B}} \psi_{m+1} \qquad 2.21$$

For perpendicular incidence ($\emptyset_{inc}$= 0), which is the first case treated historically,

$$\frac{d\psi_m}{d\zeta} = -j\frac{\alpha}{2}(\psi_{m-1} + \psi_{m+1}) \qquad 2.22$$

Now, recall the recurrence relation for Bessel functions,

$$\frac{dJ_m(x)}{dx} = \frac{1}{2}[J_{m-1}(x) - J_{m+1}(x)] \qquad 2.23$$

Then, writing ψ_m=(-j)^m B, where B= $J_m(\alpha\zeta)$, we recognize, with $\psi_m = \psi_{inc}\,\zeta_{m0}$ at ζ=0 that the amplitude of the various scattered orders is given by [**1**]:

$$\psi_m = (-j)^m \psi_{inc} J_m(\alpha\zeta) \qquad 2.24$$

Equation (2.24) represents Raman-Nath solution.

The diagram of Raman-Nath diffraction can be shown in Fig. (2.2) [**17**].

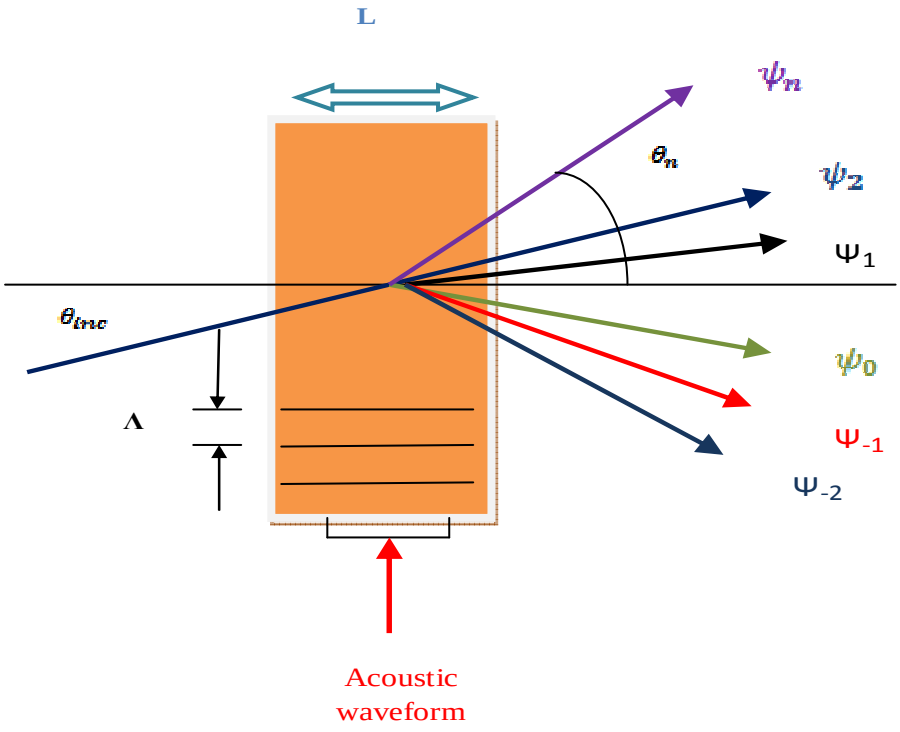

Figure (2.2): Raman-Nath diffraction [**17**].

2.5 characteristics of The Diffracted Light

There are two types of light interaction with matter these are [**22**]:

I *Isotropic Interaction*

An isotropic interaction is also referred to as a longitudinal-mode interaction. In such a situation, the acoustic wave travels longitudinally in the crystal, the incident and diffracted light beams have the same refractive index. This is a situation of great symmetry and the angle of incidence is found to match the

angle of diffraction. There is no change in polarization associated with the interaction. These interactions usually occur in homogenous crystals. In the isotropic situation, the angle of light incidence must be equal to the Bragg angle [**22**], i.e.

$$\theta_B = \frac{\lambda \mathrm{f}}{2v} \qquad 2.25$$

where $\lambda = \frac{\lambda_o}{n}$, f is the frequency of incident light, and v is the velocity of incident light.

The diagram of isotropic case is shown in Fig. (2.3) [**22**].

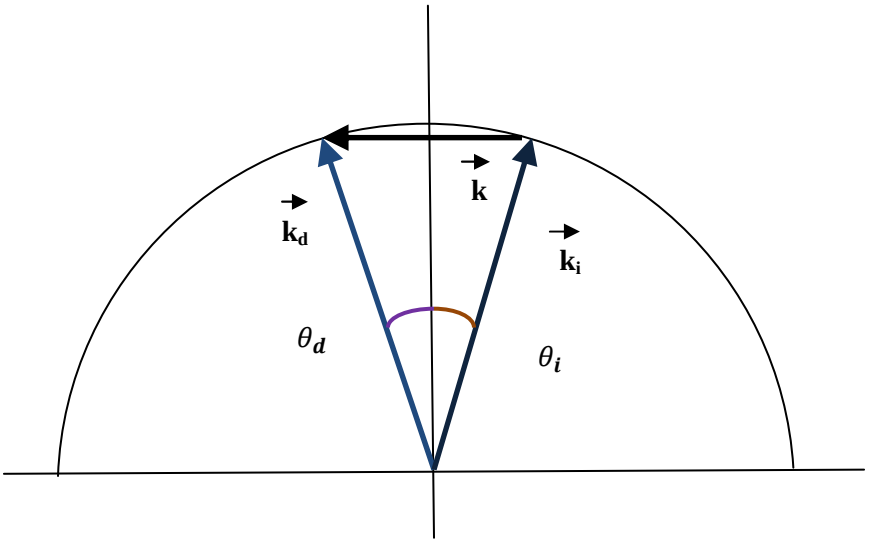

Figure (2.3): the isotropic case [**22**].

where $\mathbf{k_i} = \frac{2\pi \boldsymbol{n_i}}{\lambda_o}$ is the wave vector of the incident beam, $\mathbf{k_d} = \frac{2\pi \boldsymbol{n_d}}{\lambda_d}$ is the wave vector of diffracted beam, and $\mathbf{K} = \frac{2\pi \mathrm{f}}{\boldsymbol{v}}$

$\mathbf{n_i}$ and $\mathbf{n_d}$ are unit vectors in the incidence and diffracted direction respectively.

II Anisotropic interaction

On the other hand, in an anisotropic interaction, the refractive index of the incident and diffracted beams will be different due to change in polarization associated with the interaction. The same asymmetry which causes the difference in refractive indices also causes the acoustic wave to travel in a "shear-mode" Anisotropic interaction generally offer an increase in efficiency of the acousto-optic waves. The acoustic and optical bandwidths are used in large aperture devices [**22**]. The diagram of anisotropic case is shown in Fig. (2.4) [**22**].

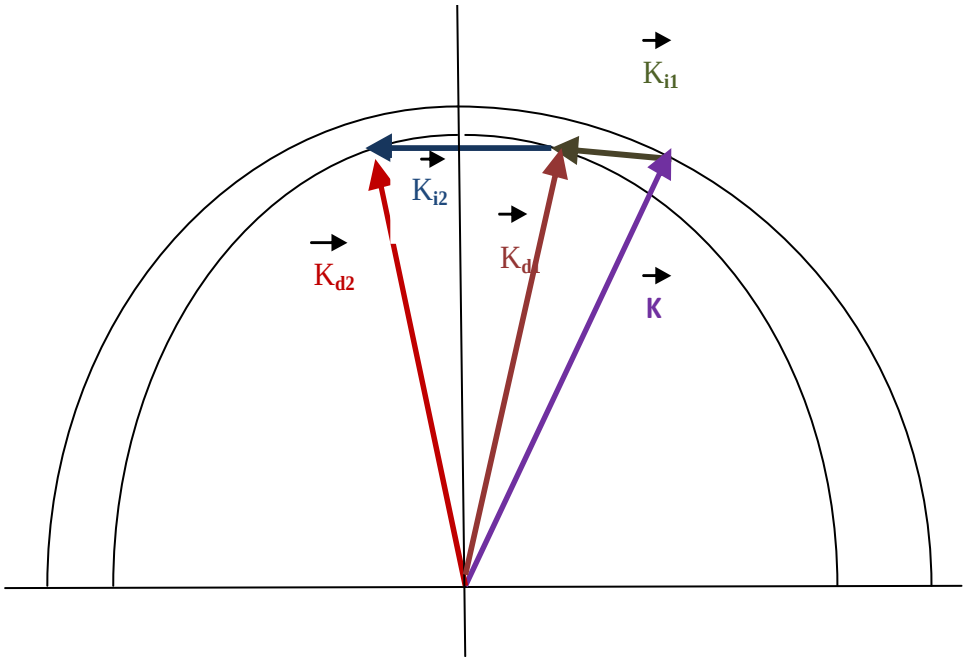

Figure (2.4): anisotropic case [**22**]

2.6 Acousto-Optic Modulation

Acousto-optic "AO" or elastic-optic effects are used to show that the refractive index of a medium is being changed either by a mechanically applied strain or by ultrasonic waves. Acousto-Optic Modulator "AOM" consists of a

medium whose refractive index undergoes a sinusoidal variation in the presence of an externally applied ultrasonic signal. There are many materials such as water, quartz, and lithium-niobate that exhibit changes in the refractive index once they are subjected to strain. The variation in the acoustic wave velocity is negligible; therefore, it could be possible to assume that the variation of refractive index in the medium is stationary, as far as, the optical wave front is concerned. A narrow beam of incident light on the medium is scattered into primary diffraction orders. Higher diffraction orders have negligible intensities associated with them. The zero-order has the same frequency as the incident beam, while the frequencies of "+1" and "-1" orders undergo frequency modulation [**23**].

In order to appreciate the basics of AO effect, we can consider the collisions of photons and phonons. Light consists of photons that are characterized by their momentum $\hbar k_a$ and $\hbar k_1$, respectively, where k_a and k_1 are the wave vectors of photons and phonons, respectively. Photon and phonon energies are given by hf_a and hf_1, respectively, where f_a and f_1 are the frequencies of photon and phonon, respectively. The condition for the conservation of momentum when applied to this collision is given by following equation [**23**]

$$k_1 \cos\theta = k_1' \cos\theta' \qquad 2.26$$

and

$$k_a = k_1 \sin\theta + k_1' \sin\theta' \qquad 2.27$$

where θ is the angle of incident photon, and θ' is the angle of scattered photon, θ' Can be evaluated by [**23**]

$$\theta' = tan^{-1}[\frac{k_a}{k_1}\sec\theta - \tan\theta] \qquad 2.28$$

Fig.(2.5) shows the schematic diagram of photon-phonon collision resulting in the annihilation of a phonon [**23**].

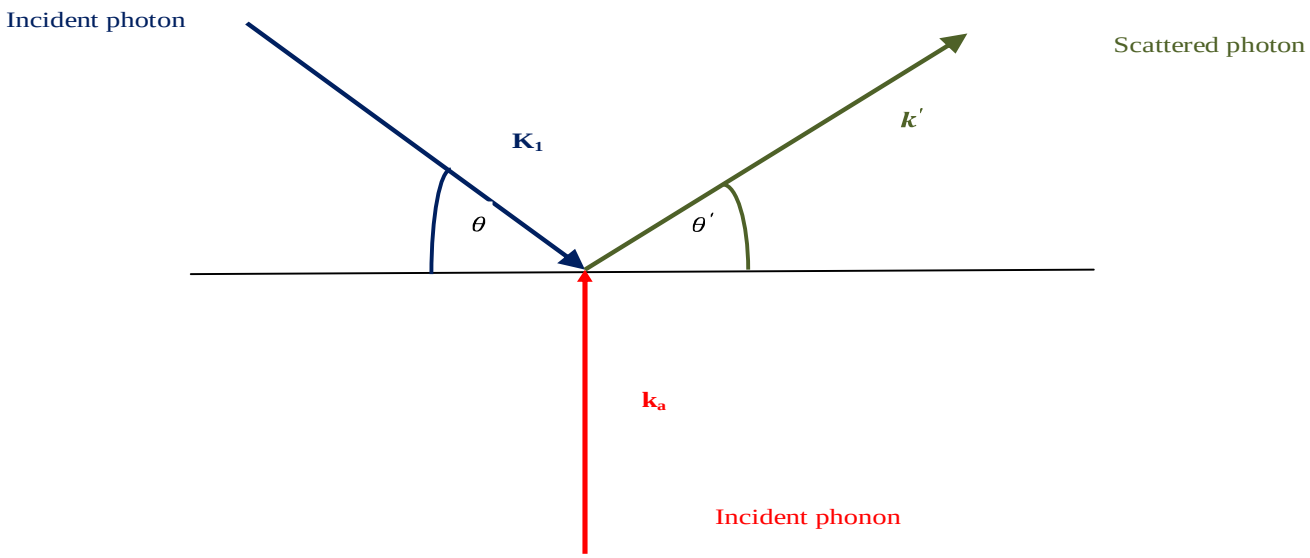

Figure (2.5): photon-phonon collision resulting in the annihilation of a phonon [**23**]

In isotropic medium $\theta = \theta'$and $k_1 = k_1'$.

At this particular, angle of incidence referred to the Bragg angle, photon momentum is conserved and the diffraction efficiency reaches a maximum. It is important to realize that the acousto-optical effect is produced by multiple collisions of photons and phonons. The condition for conservation of energy is

only approximately valid in photon-phonon collision. However, in practice, the frequency of the scattered photon $f_{a=}f_a^{/}$, since $f_1 \ll f_a$.

In anisotropic materials, k_1' approaches rk_1, where r is the ratio of the refractive indices corresponding to the diffracted and incident waves, respectively. Equations (2.26) and (2.27) can be modified to give [**23**].

$$\theta = sin^{-1}[\frac{k_a}{2k_1}\{1 + \left(\frac{k_1}{k_a}\right)^2(1 - r^2)\}] \qquad 2.29$$

and

$$\theta' = sin^{-1}[\frac{k_a}{2rk_1}\{1 - \left(\frac{k_1}{k_a}\right)^2(1 - r^2)\}] \qquad 2.30$$

Notice that $\theta = \theta'$ only when $r = 1$, because it is not possible to have $r = \left(\frac{k_a}{k_1}\right) - 1$ when $k_a \ll k_1$. The phenomenon $\theta = \theta'$ is associated only with the Bragg angle of incidence and the condition $r = 1$. This means, there are two values of "k_a" and "k_1'" that satisfy the condition of momentum conservation. Note that in anisotropic media, the momentum conservation is satisfied over a wider rang of acoustic frequencies or incident light beam than in isotropic materials. Note that, the power in the scattered beam varies with θ and reaches a maximum when θ is equal to the Bragg angle. In Raman-Nath regime, the coustic-optic grating can be treated as a simple grating. Such that [**23**]:

$$m\lambda = \lambda_a sin\theta_m \qquad 2.31$$

By comparison, in the Bragg regime the acoustic field acts very much like a "thick" diffraction grating requiring that [**23**]:

$$\theta = \theta' = sin^{-1}(\frac{m\lambda}{2\lambda_a}) \qquad 2.32$$

A Bragg cell can be used to switch light beam directions by turning on and off the acoustic source. The intensity of the diffracted light depends on the amplitude of the acoustic wave. Therefore, an amplitude modulation of the acoustic wave will produce amplitude-modulated light beams.

When compared with an electro-optic modulator "EOM" that consumes voltage on the order of 10^3 V. An AOM requires only a couple of volts. But the propagation of the acoustic wave is slow in the medium [**23**].

2.7 **Acousto-Optic Devices** (AOD)

An AOM is a device which can be used for controlling the power, frequency or spatial direction of a laser beam with an electrical drive signal. It is based on the AO effect, i.e. the modification of the refractive index by the oscillating mechanical pressure of a sound wave. AOM sometimes called Bragg cell. The scattered beam has slightly modified optical frequency and a slightly different direction. Because the wave number of the sound is very small compared with that of the light beam there are three kinds of AO these are [**24**]:

I Acousto-Optic Modulator (AOM)

The Acousto-Optic Modulator is based on the elasto-optic effect, in which a material strain causes a change in the refraction index of the material. When the strain is generated by an acoustic compression or rarefaction, an AOM is formed. Because the acoustic signal is sinusoidal, a moving refractive index

grating is formed in the device. Like a permanent grating, the various wavelengths are spatially diffracted and separated from each other. With an output coupler placed at the appropriate diffraction order location, tunable filtering and switching can be achieved [**25**].

II Acousto-Optic Filter (AOF)

The principle behind the operation of AO filters is based on the wave length of the diffracted light being dependent on the acoustic frequency. By tuning the frequency of the acoustic wave, the desired wave length of the optical wave can be diffracted acousto-optically. There are two types of the AO filters, the collinear and non-collinear filters [**25**]

III Acousto-Optic Deflectors (AOD)

An AO deflector spatially controls the optical beam. In the operation of an AOD the power driving the acoustic transducer at a constant level, while the acoustic frequency is varied to deflect the beam to different angular positions. AODs are essentially the same as AOMs, In an AOM only the amplitude of the sound wave is modulated, while in the AOD both the amplitude and frequency are a adjusted [**25**].

2.8 Multichannel Acousto-Optic Modulators (MAOM)

The AOM involve a single transparent crystal "TeO_2" operated in the slow shear mode. At one end of the crystal is an ultrasonic transducer, which converts the electrical signal to an acoustic wave that is launched down the crystal. As the propagation of the acoustic wave, the regions of the elastic shear present a

modulated the refractive index to the optical beam, that passes perpendicularly to the acoustic wave.

The optical beam, thus, emerges from the crystal with a relative phase difference across its width which is proportional to the amplitude of the acoustic wave along the length of the crystal [**26**].

The multichannel of acousto-optic modulator can be shown in Fig. (2.6) [**26**].

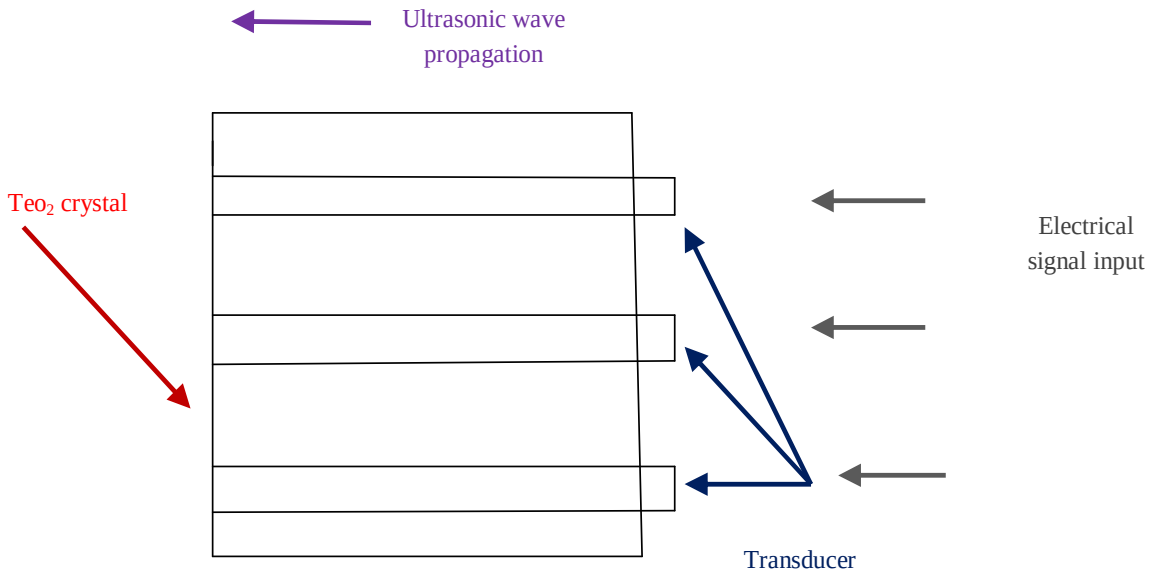

Figure (2.6): The multichannel Acousto-Optic Modulator [**26**]

2.9 Modern Application of Acousto-Optic Effect

There are several applications of the AO effect, in this study we will consider the following [1]:

2.9.1 Intensity Modulation of a Laser Beam

This application represents the popular application for an acousto-optic Bragg cell. By changing the amplitude of the sound, i.e. through peak phase delay "α" can achieve intensity modulation of the diffracted beam. In fact, it has the ability to modulate laser light [**27**]

The diagram of the zeroth and first orders intensity diffraction curves plotted as a function of α are shown in Fig. (2.7) [**27**].

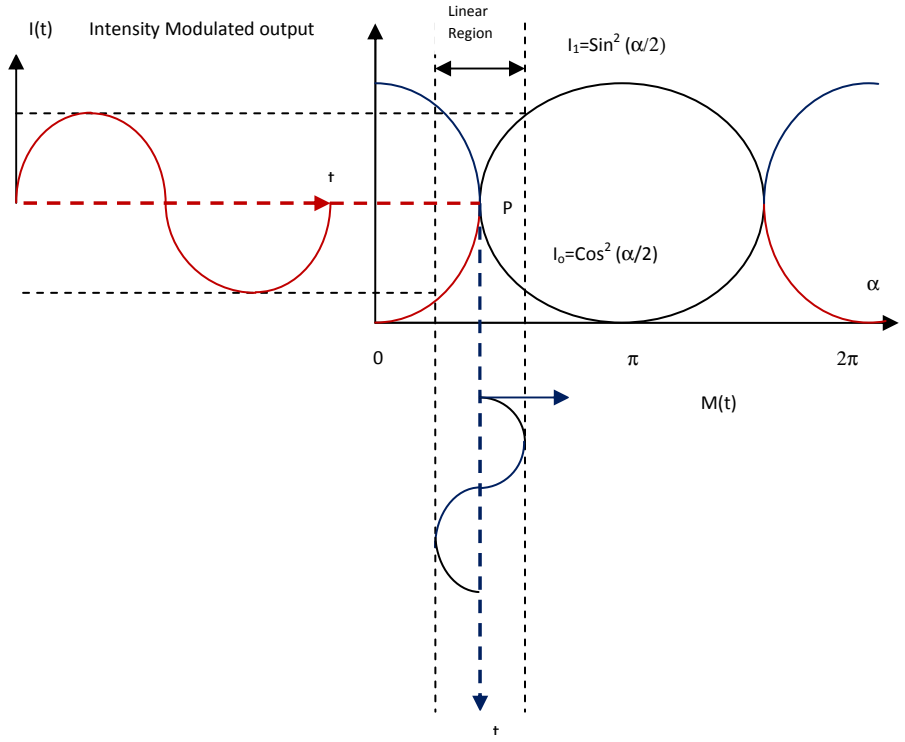

Figure (2.7) The zeroth and first order intensity diffraction curves plotted as a function of α [**27**]

These curves illustrates the relationship between the modulating signal “m (t)” and the intensity modulated output signal “I (t)”, where m (t) is biased along the linear portion of the first order diffraction curve. The intensity modulation can be obtained by using the zeroth diffracted order. However, the two diffracted orders process information in the linear regions with opposite slopes. That is lead to any demodulated electrical signal received by the first diffracted will be 180 degree out of phase with the electrical signal received by the zeroth diffracted order [**27**].

The experimental setup for “AM-demodulation” is shown in Fig. (2.8) [**27**].

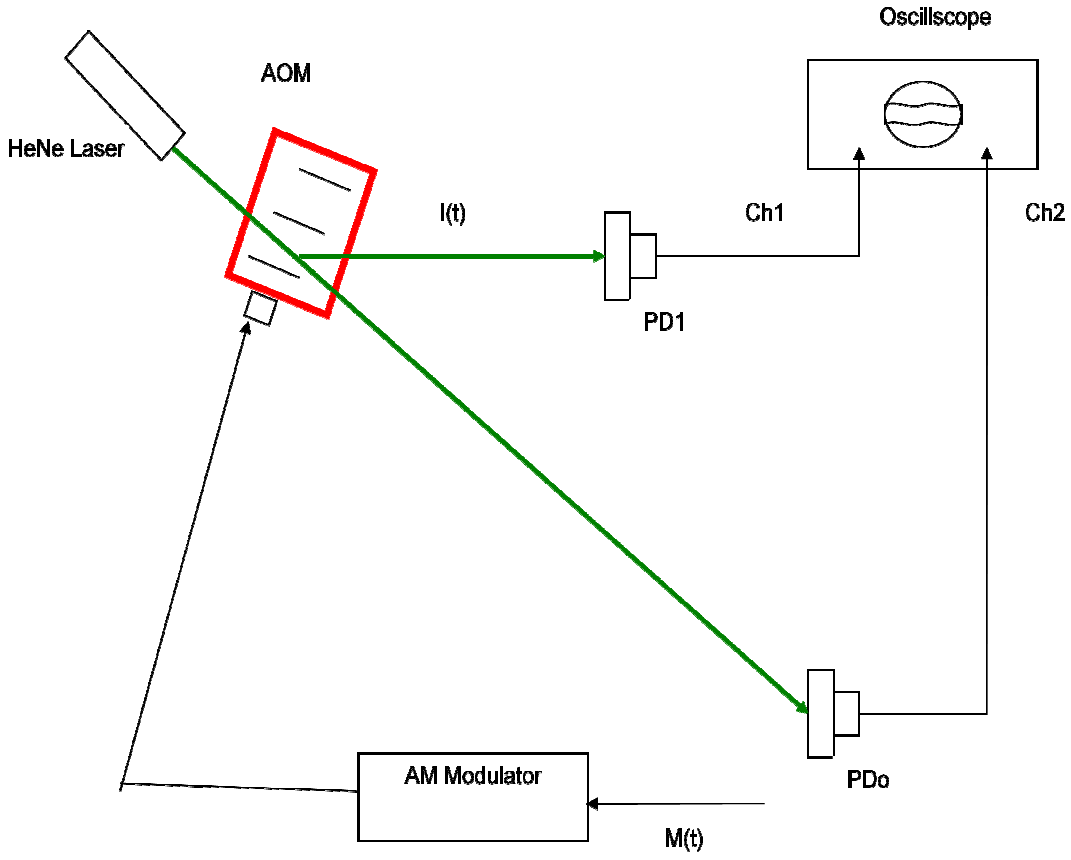

Figure (2.8) An experimental setup for “AM-demodulation” [**27**]

where AM is the amplitude modulation, the amplitude of the modulating signal is given by [**27**]:

$$[b + m(t)]\cos(\Omega t) \qquad 2.33$$

Where "b" is a constant and Ω is the center frequency of the acoustic transducer.

The output of the two photo detectors PD_0 and PD_1 of the audio and electrical signals are shown in Fig. (2.9) [**27**].

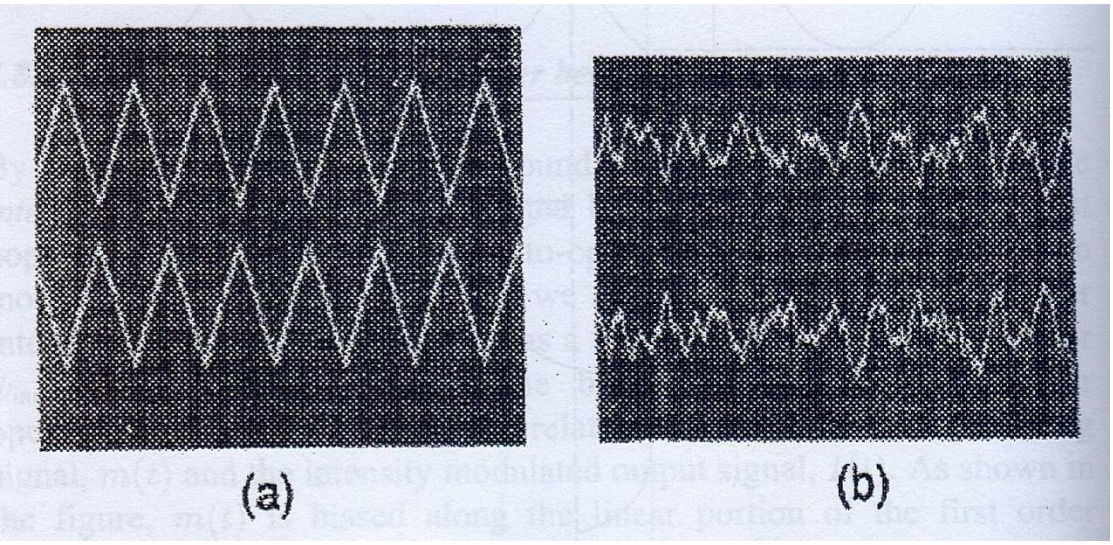

(a) triangular (b) Audio

Figure (2.9): (a) the output of the two photo detectors **PD_0** and **PD_1**,(b) the two 180 degree out of phase detected electrical signals [**27**]

2.9.2 Light Beam Deflector and Spectrum Analyzer

The amplitude of the modulating signal is varied therefore; the frequency of the modulating signal is changed for applications in light deflection. The angle

between the first order beam and the zeroth order beam is called the deflection angle "$\emptyset_d$" and is given by [**1**]:

$$\Delta\emptyset_d = \Delta(2\emptyset_B) = \frac{\lambda_0}{2\pi V_s}\Delta\Omega \qquad 2.34$$

where $\Delta\emptyset_d$ is the change in the deflection angle, $\Delta\Omega$ is the change of the sound frequency, and V_s is the sound velocity.

The diagram of light beam deflector where the acousto-optic modulator operates in the Bragg regime is shown in Fig. (2.10) [**1**].

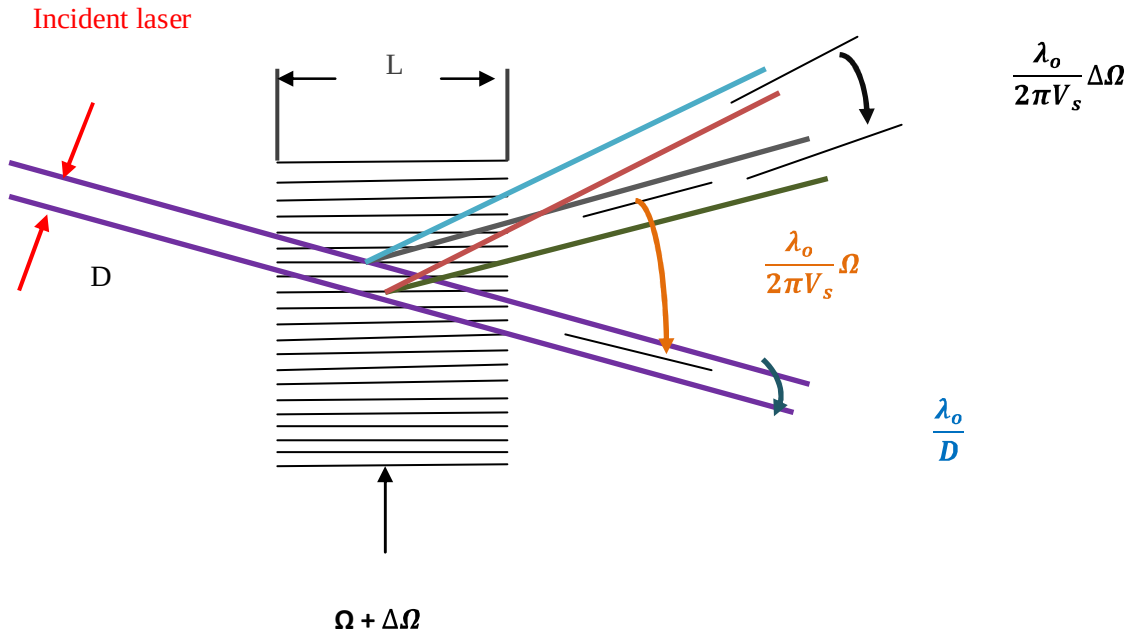

Figure (2.10): a light beam deflector where the AOM operates in the Bragg regime [**1**]

Instead of a single frequency input, the sound cell can be addressed simultaneously by a spectrum of frequencies. The Bragg cell scatters light

beams into angles controlled by the spectrum of acoustic frequencies as each frequency generates a beam at a specific diffracted angle. Because the acoustic spectrum is identical to the frequency spectrum of the electrical signal, the device essentially acts as a "*spectrum analyzer*" [**1**].

2.9.3 Demodulation of Frequency Modulated "FM" Signals

In this section, we discuss how to make use of the Bragg cells frequency-selecting capability to demodulate frequency modulated "FM" signal. The *i*-th FM station is beamed, in a direction relative to the incident beam is given by [**28**].

$$\emptyset_{di} = \frac{\lambda_0 \Omega_{0i}}{2\pi V_s} \qquad 2.35$$

where $\emptyset_{di}$ is the deflection angle at *i*-th FM station, and Ω_{0i} is the spectrum of carrier frequency, *i*=1, 2…

The Principle of the FM demodulation is that the actual instantaneous angle of deflection deviates slightly from Equation (2.35) due to the inclusion of $\Delta\Omega_i(t)$, that causes a "Wobble" $\Delta\emptyset_{di}(t)$ in the deflected beam. In particular, $\Delta\emptyset_{di}(t)$ is given by [**28**]

$$\Delta\emptyset_{di}(t) = \left(\frac{\lambda_0}{2\pi V_s}\right)\Delta\Omega_i(t) \qquad 2.36$$

Ministry of Higher Education and Scientific Research

AL-Nahrain University

College of Science

Department of Physics

COMPUTER SIMULATION OF AN ACOUSTO-OPTICAL DEVICE FOR PHOTONIC SYSTEM

A THESIS SUBMITTED TO THE COLLEGE OF SCIENCE, AL-NAHRAIN UNIVERSITY IN PARTIAL FULFILLMENT OF THE RECUIREMENTTS FOR THE DEGREE OF MASTER SCIENCE IN PHYSICS

BY

MARWA KAMAL MUSTAFA

B.Sc

2008

The Supervisors

Prof. Dr. Ayad A. Al-Ani **Dr. Ahmad K. Ahmad**

Dec. 2010 **1431**

We certify that this thesis was prepared under our supervision at the Al-Nahrain University as a requirement for the degree of master science in physics.

Signature:

Name : Dr. Ayad A. Al-Ani

Title : Professor

Address: Department of Physics

College of Science

Al-Nahrain University

Date : / /2010

Signature:

Name : Dr. Ahmad K. Ahmad

Title : Assistant Professor

Address: Department of Physics

College of Science

Al-Nahrain University

Date : / /2010

In view of the available recommendation, I forward this thesis for debated by the examination committee.

Signature:

Name : Dr. Salah A.H. Saleh

Title : Assistant Professor

Address: Head of Physics

Department

College of Science

Al-Nahrain University

Date : / /2010

LIST OF CONTENTS

LIST OF CONTENTS

List of Figures

List of Tables

NOMENCLATURE		
$E_{inc\ (r,t)}$	Incident of the electric field	
f_a	Frequency of phonon	Hz
F_a	Acoustic frequency	Hz
J	Complex number	
k_0	Wave vector of incident plane wave of light $\mathbf{ko} = \frac{2\pi}{\lambda}$	
k_1	Wave vector of phonon	
k_{+1}	Wave vector of diffracted or scattered plane wave of light $\boldsymbol{k_{+1}} = \frac{2\pi}{\Lambda}$	
k_a	Wave vector of photon	
k_d	Wave vector of the diffracted beam = $\frac{2\pi n_d}{\lambda_d}$	
k_i	Wave vector of incident beam = $\frac{2\pi n_i}{\lambda_o}$	
P_a	Power of acoustic wave	watt
T	Time propagation	sec
V_a	Acoustic velocity	m/s
w_0	Angular frequency of the light incident	Hz
w_{+1}	Angular frequency of the scattered light	Hz
Greek Symbols		
λ_0	Wave length of the light	m
Λ	Wave length of the acoustic wave	m
Ω	Angular frequency of the sound	Hz
Θ	Diffraction angle of light	degree
$ø_{inc}$	Incident angle of light	degree
μ_o	Permeability of the material	h/m
ϵ	Permittivity of the material	f/m
Ψ	Normalized intensity of the diffracted order	
α	Peak phase delay	
$\boldsymbol{\zeta}$	Normalized distance inside the acousto-optic cell	

References:

1- Poon, T. and Kim, T.: “Engineering Optics with MATLAB”, World Scientific Publishing Co. 2006.

2- Herrman, H.: “Integrated Optical Devices in Lithium Niobate”, Optics and Photonics News, **19**, pp. (24-31), 2008.

3- Neos Technologies: “Introduction to Acousto-Optic Modulators and Deflectors”, A Gooch and Housego Company 2000.

4- Vivek, V.: “The Acousto-optic Modulator”, Optical Switches, 1999.

5- http:/www. Google.Com/Acousto-Optics-70 Years After First Ultrasonic Light Diffraction Experiments, 1980.

6- Adrianus, K.: “Two-Dimensional Plane Wave Theory of Strong Acousto-Optic Interaction in Isotropic Media”, Optical Society of America, **69**, pp. (678-683), 1979.

7- Fox, A.J.: “A plane Wave Derivation of the Bragg Acousto-Optic Equations and Their Applications to The Scattering of Finite-Width Optical Beams”, Optical and Quantum Electronics, **14**, pp. (189-200), 1982.

8- Zadorin, A.S. and Sharangovich, S.N.: “Strong Acousto-Optic Interaction in the Field of A focused Acousto-Optic Wave”, Institute of Automated Control System and Radio Electronics, Tomsk, **29,** No.7, pp. (798-808), 1987.

9- Brooks, P. and Reeve, C.D.: “Limitation In Acousto-optic FM Demodulators”, IEEE Proc. Opto-Electron, **142**, No.3, pp. (149-156),1995.

10- Sharangovich, S.N.: “Diffraction Characteristics of Acousto-Optic Interaction in an Acoustic Field with A curved Wave Front”, Russian Physics Journal, **38,** No.4, pp. (41-50), 1995.

11- Thompson, C. and Weiss, B.L.: “Acousto-Optic Bragg Diffraction in

Si Ge/Si Planer Waveguides”, IEEE Proc. Opto-Electron, **143**, No.5, pp. (303-306), 1996.

12- Dunn, D., Xia, J. and Poon, T.: “Three-Dimensional Analytical and Numerical Solutions for Acousto-Optic Interaction”, Southeastern Symposium on System Theory (SSST 97), pp. (488), 1997.

13- Dunn, D.: “Real-Time Image Processing Using Acousto-Optic Bragg Diffraction”, Blacksburg, Virginia, PhD. Thesis, 1998.

14- Cont, A. and Poon, T.C.: “Simulation of Bistable Acousto-Optic Devices Using MATLAB”, Virginia, IEEE Southern Symposium on System Theory (SSST), pp. (296-298), 2003.

15- Masalsky,N.: “Waveguide Acousto-Optical Units for Correlation and Spectrum Processing of Multi-Color Optical Signals in Real Time”, Russian Academy of Science, IEEE CAOL, pp. (292-301), 2003.

16- Huang, D., Liao, C., Wei, C. and Li, P.: “Simulations of Opto-Acoustic Wave Propagation in Light Absorbing Media Using the Finite Difference Time Domain Method”, Department of Electrical Engineering, National

Taiwan University, IEEE International Ultrasonic, Ferroelectrics and Frequency Control Joint 50th Anniversary Conference, pp. (1856-1859), 2004.

17- Al-Obaidy, H.: "Construction of An Acousto-Optic Deflector and Its Application in Bistable Devices", University of Technology, Iraq, MS.C Thesis, 2005.

18- Tsarev, A.: "Finite Difference Time Domain simulation of Compact Acousto-Optic Filters Based on Multi-Reflection Beam Expanding", Siberian, Branch of the Russian Academy of Sciences, Quantum Electron **37**, pp. (393-398), 2007.

19- Molchanov, V. and Makarov, O.: "Quasi-Collinear Acousto-Optic Filters Using Strong Acoustic Anisotropy in Tellurium-Dioxide Crystal", Technological University, Russia, Journal of Physics: Conference series 92, pp. (1-4), 2007.

20- Baryshev,V.N. and Epikhin,V.M.: "Compact Acousto-Optic Modulator Operating in the Purely Raman-Nath Diffraction Regime as a Phase Modulator in FM Spectroscopy", Institute of Physico-Technical and Radio Measurements, State Scientific Center, Russian Federation, Quantum Electron, 40, PP. (431), 2010.

21- Haupt, R.L.: "Engineering Electro Magnetic Application", Taylor and Francis Group 2006.

22- Oliveira, R.A., Neves, P.T., Pereira, J.T., Pohl, A.A.P.: "Numerical Approach for Designing a Bragg Grating Acousto-Optic Modulator Using the

Finite Element and the Transfer Matrix Methods", Fedral University of Technology, Brazil, Optics Communication, **281**, pp. (4899-4905), 2008.

23- Malacara, D. and Thompson, B.: "Hand Book of Optical Engineering", Marcel Dekker, New York 2001.

24- paschotta, R.: "Encyclopedia of laser Physics and Technology", 2008.

25- Yariv A., Yeh P.: "Optical Waves in Crystals: Propagation and Control of Laser Radiation", Wiley Inter-science Publication, pp. (366-387), 1984.

26- Bademian, L.: "Parallel- Channel Acousto-Optic Modulation", Optical Engineering, **25**, pp. (303-308), 1986.

27- Poon, T.C., Meneill, M.D. and Moore D.J.: "Two Modern Optical Signal Processing Experiments Demonstrating Intensity and Pulse-Width Modulation Using an Acousto-Optic Modulator", American Journal of Physics, **65**, pp. (917-925), 1997.

28- Poon, T.C. and Pieper, R.J.: "An Acousto-Optic FM Receiver Demonstrating Some Principles of Modern Signal Processing", IEEE Trans. on Educations, **27**, No.3, pp. (11-17), 1985.

29- Farlow, S.: "Partial Differential Equation for Scientists and Engineers", University of Maine, 1937.

30- WWW.ISOMET.Com.

31- Taflove, A.: “Application of the Finite Difference Time Domain Method to Sinusoidal Steady State Electro Magnetic Penetration Problem”, IEEE Transaction on Electro Magnetic Compatibility, pp. (191-202), 1980.

32- Garcia, G., Bretones, R., Olmedo, G. and Martin, G.: “Finite Difference Time Domain Methods” Department of Electro magnetism and Matter Physics, University of Granada, Microwave and Optical Technology Letters, pp. (414-416), Spain, 2001.

33- Wu, Y. and Wassell, I.: “Introduction to the Segmented Finite Difference Time Domain Method”, Computer Laboratory, University of Cambridge, IEEE transactions on Magnetics, **45,** No.3, pp. (1364-1367), 2009.

34- Yee, K.: “Numerical Solution of Initial Boundary Value Problems Involving Maxwell’s Equations in Isotropic Media”, IEEE transactions on Antennas and Propagations, **14**, pp. (302-307), 1996.